ORIGINAL PAPER

Damage constitutive model and meso-failure characteristics of freeze–thaw rock under triaxial compression

Qiang Feng[1] · Jiansheng Xu[1] · Changxi Cai[1] · Weiwei Liu[1] · Jichao Jin[1] · Weiwei Han[1] · Zhe Qin[1]

Abstract

In order to evaluate the damage deterioration degree of freeze–thaw rock under in-situ stress in cold area engineering, it is necessary to establish the triaxial compression damage constitutive model and study on meso-failure characteristics of freeze–thaw rock. The triaxial compression tests under confining pressure of 3 MPa, 5 MPa, and 10 MPa were carried out on saturated sandstone after 0, 20, 40, and 60 freeze–thaw cycles. The results show that with the increase of freezing–thawing times, the peak deviatoric stress and elastic modulus under the same confining pressure decrease gradually, and increase gradually with the increase of confining pressure. The triaxial compression damage constitutive model of freeze–thaw rock was established based on the dissipation energy ratio and the principle of minimum energy dissipation. Based on this model, the evolution law of energy ratio in different stages of compression process was studied, and the influence characteristics of confining pressure and freeze–thaw on rock failure were analyzed. PFC2D was used to establish the numerical method on triaxial compression of frozen-thawed rock and determine the calculation parameters. The energy evolution law and the number growth law of different cracks in the triaxial compression process of frozen-thawed rock were studied. It is found that the energy value at the peak and the ratio of tensile crack to shear crack decrease with the number of freezing–thawing cycles. Meanwhile, the characteristics of freezing–thawing cycles promoting the shear failure of rock were clarified.

Keywords Triaxial compression test · Principle of minimum energy consumption · Damage constitutive model · Energy analysis · Microscopic failure characteristics · Crack number

Introduction

With the continuous implementation of China's western development strategy, the construction of infrastructure projects in cold regions is also ongoing. Due to the freeze–thaw cycle, the surrounding rock will deteriorate (Luo et al. 2015), which may lead to instability of surrounding rock, structural cracking, and other rock engineering problems (Krautblatter et al. 2013; Pudasaini et al. 2014). It is of great theoretical and practical significance for engineering construction in cold regions to establish the triaxial damage constitutive model of rock under freeze–thaw conditions, explore the failure mechanism of rock mass after freeze–thaw damage, and identify the microscopic failure characteristics of freeze–thaw rock.

At present, many scholars have applied damage mechanics to study constitutive model and failure mechanism of freeze–thaw rock. Krajcinovic et al. (1982) established a simple and effective theoretical model by combining continuous damage theory and statistical strength theory. Wang et al. (2007) proposed a statistical constitutive model of rock damage based on Weibull distribution function, and studied the influence of different strength criteria and residual strength on the model. Wang et al. (2008) proposed a damage constitutive model of rock considering confining pressure and loading rate based on Weibull distribution. Zhang et al. (2013) defined the plastic internal variable by analyzing the coupling relationship between elastic deformation and plastic deformation, and proposed a damage constitutive model to describe the elastic–plastic behavior of porous rock. Tian et al. (2014) established a damage statistical constitutive equation based on strain equivalent hypothesis and Lade-Duncan criterion. Zhao et al. (2016) established a new

✉ Weiwei Liu
  skd994491@sdust.edu.cn

1   Shandong Key Laboratory of Civil Engineering Disaster
    Prevention & Mitigation, School of Civil Engineering
    and Architecture, Shandong University of Science
    and Technology, Qingdao 266590, China

quasi-brittle rock damage constitutive model based on a new damage tolerance principle.

In recent years, many scholars have also used energy theory to study the damage constitutive relationship and failure mechanism of rock (Chen et al. 2019; Meng et al. 2019). Li et al. (2019) coupled the dissipation function with the damage variable to establish the elastoplastic damage constitutive model of frozen soil. Liu et al. (2016) proposed a damage constitutive model based on the principle of energy dissipation, which can well describe rock compaction and rock behavior under cyclic loading. According to the energy dissipation principle and crack closure effect, Wen et al. (2018) established a damage constitutive model which can reflect the deformation damage evolution of rock during the crack closure stage. Pan et al. (2020) combined the damage statistical method and energy theory to divide the rock into skeleton and void, and established a nonlinear statistical damage constitutive curve based on Weibull distribution function. The principle of minimum energy consumption is an important part of energy theory, which can well reveal the damage evolution law of rock. However, there are few studies on the damage evolution of freeze–thaw rock under triaxial compression using this principle.

With the development of numerical simulation methods, rich achievements have been achieved in the study of rock damage evolution and constitutive mode. Chen et al. (2016) simulated the damage evolution process of triaxial compression test and predicted the damage and ultimate state of rock using the discrete element model characterized by Voronoi block. Rakhimzhanova et al. (2019) used DEM to simulate triaxial compression test and studied the relationship between strength parameters and bond strength. Qiu et al. (2020) established concrete constitutive model under freeze–thaw condition based on plastic damage theory. Zhu et al. (2021) proposed a new model to simulate the damage evolution of freeze–thaw rock based on DEM, which simplified the rock samples into contact particle sets. Zhang et al. (2021) used PFC^{3D} to simulate the triaxial compression process of sandstone and analyzed the damage process and energy evolution law. Guo et al. (2021) established the triaxial compression numerical model of rock based on COMSOL multiphysics software, which can simulate the damage evolution of brittle rock. Therefore, the numerical simulation research on the energy evolution and crack number evolution of freeze–thaw rock under triaxial compression needs to be further enriched.

Triaxial compression tests of saturated sandstone specimens after freeze–thaw cycles were carried out in this paper. Based on the principle of minimum energy dissipation and dissipation energy ratio, the coupled damage constitutive model under the combined action of freeze–thaw and load was established, and the correctness of the model was verified by comparing with the test curve. Based on this constitutive model, the energy ratios in the whole process of rock compression to

Table 1 The average parameters of rock samples

Parameter	Density (g/cm^3)	Porosity (%)	Permeability (mD)	P-wave velocity (m/s)
Average value	2.34	9.80	2.40	2970

Fig. 1 Rock samples

failure were studied. In this paper, the law of energy evolution and crack development during the triaxial compression of freezing–thawing rock was analyzed by using the newly established numerical simulation method. The role of freeze–thaw cycle in rock failure process was also discussed.

Test method and results

Processing and screening of rock samples

The experimental material is yellow sandstone, and the whole rock is processed into φ50 mm × 100-mm cylindrical rock sample, and the accuracy is controlled within ± 0.3 mm. The accuracy of nonparallelism at both ends is within ± 0.05 mm. After processing, the surface-damaged rock samples were removed through visual observation, and then the uniformity of the sandstone was checked by testing the density, porosity, permeability, and p-wave velocity of the rock samples. The specific test data are shown in Table 1. Finally, the test samples are selected as shown in Fig. 1.

XRD and SEM tests

XRD test steps and results

The Rigaku X-ray powder diffractometer, manufactured by Neki Corporation of Japan, was used in the XRD test,

and its accuracy was 1/10,000°. The energy spectrum obtained by XRD test was shown in Fig. 2. Phase analysis based on the test results shows that α-quartz content is high, accounting for 83.6%. The remaining components are relatively small, including 1.2% of stishovite, 2.3% of α-squamous quartz, 3.8% of β-squamous quartz, and 9.1% of kaolinite.
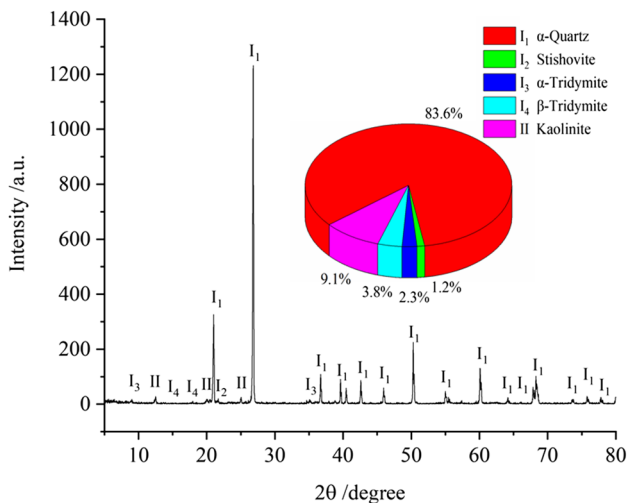

**Fig. 2** Energy spectrum and mineral composition content

SEM test steps and results

Scanning electron microscopy (SEM) was performed using Apreo S HiVac high-resolution scanning electron microscopy (SEM) produced by Simmerfel Technology Company of USA. The sandstone samples were divided into two groups by angle mill. One group was made of block samples with length, width, and height less than 1 cm. The other group grinds into powder particles. The block samples were placed on both sides of the loading platform and bonded with insulating tape. The powder particles were smeared on the insulating tape in the middle. The surface of the block sample was observed with $1000\times(100\ \mu m)$ and $2000\times(50\ \mu m)$ lenses, and the powder particles were observed with $15,000\times(10\ \mu m)$ and $30,000\times(5\ \mu m)$ lenses. The test results were shown in Fig. 3. It can be seen that the sandstone has dense texture and obvious layered structure characteristics.

Freeze–thaw cycle test

The experiment simulated the temperature at the location of Yuximolegai Dasan in Tianshan Mountains, China. According to the monitoring data of China Meteorological Administration, the freeze–thaw cycle temperature range of this test was finally determined to be $-30\sim30$ °C. The rising and cooling rate of the high- and low-temperature alternating test

Fig. 3 SEM results

(a) 1000× (100μm)

(b) 2000× (50μm)

(c) 15000× (10μm)

(d) 30000×(5μm)
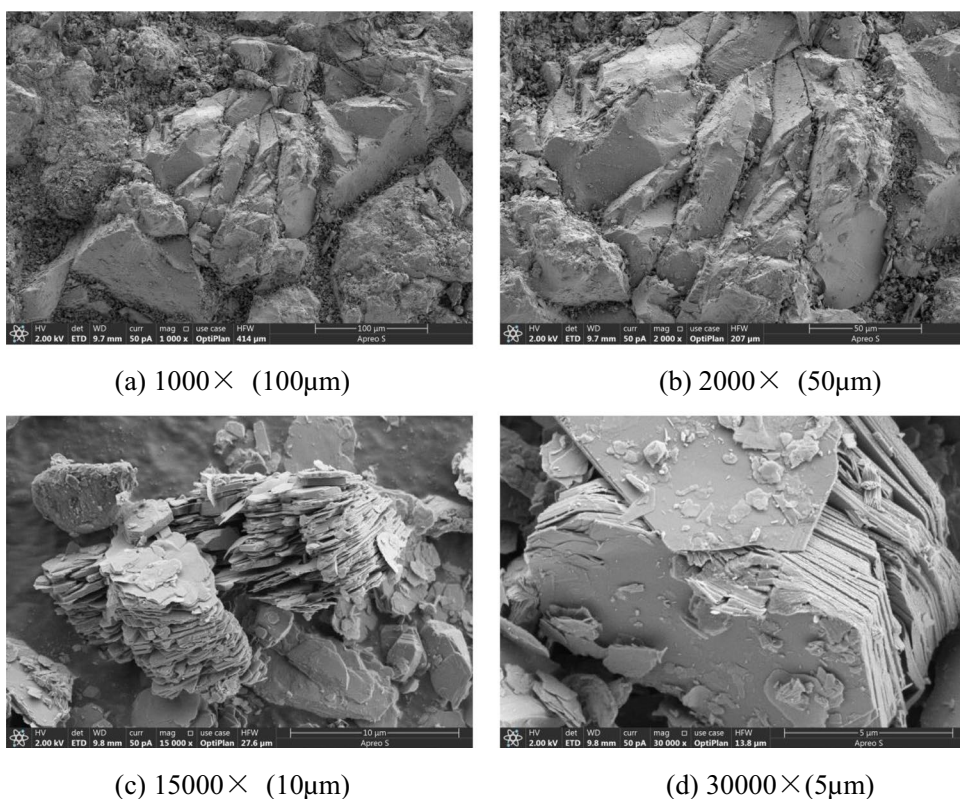
chamber used is 1~3 °C/min. Through the temperature test of the central location of the rock, it is known that the freezing process of the rock takes 4 h, the melting process takes 4 h, and the total time required for this freeze–thaw cycle is 9 h. Freeze–thaw time–temperature curve (as shown in Fig. 4) is consistent with that in the literature (Feng et al. 2022). The saturated rock specimens were put into the freeze–thaw test instrument for 0, 20, 40, and 60 freeze–thaw cycles. After the freeze–thaw cycle was over, the rock samples were taken out for sealed storage, avoiding contact with water in the air to ensure subsequent test results.

Triaxial compression test

TAW-2000 electro-hydraulic servo control pressure testing machine was used for triaxial compression test. The axial displacement range is 30 mm and the axial pressure is 2000 kN. Triaxial compression tests with confining pressures of 3 MPa, 5 MPa, and 10 MPa were carried out on rocks after 0, 20, 40, and 60 freeze–thaw cycles. The axial compression was loaded at a rate of 0.1 mm/min until the specimen was destroyed. Twelve stress–strain curves were obtained under the combination of freeze–thaw times and confining pressure, as shown in Fig. 5. The peak deviatoric stress, peak axial strain, and elastic modulus were shown in Table 2.

The experimental results show that the peak deviatoric stress of sandstone after 0, 20, 40, and 60 freezing–thawing cycles decreases gradually under confining pressures of 3 MPa, 5 MPa, and 10 MPa. When the confining pressure was 3 MPa, it decreased 2.94%, 7.13%, and 16.47% for every 20 freezing–thawing cycles, respectively. When the confining pressure was 5 MPa, it decreased 5.44%, 5.42%, and 2.01% for every 20 freezing–thawing cycles, respectively. When the confining pressure was 10 MPa, it decreased 3.10%, 3.43%, and 3.60% for every 20 freezing–thawing cycles, respectively.
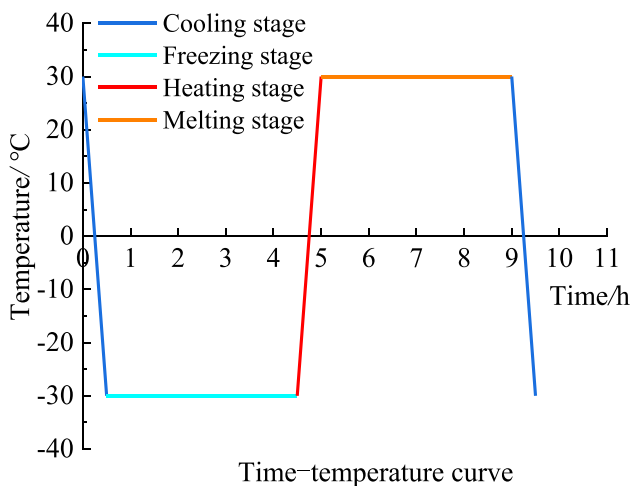

Fig. 4 Time–temperature curve of freeze–thaw cycle

When the water in the rock is frozen at low temperature, the volume expands, while the solid medium contracts when it is cold. In the interior of the rock, obvious local tensile and compressive stress will be generated, which makes the original cracks in the rock expand, and also accompanied by the generation of new cracks. Therefore, as the number of freeze–thaw cycles increases, rock damage intensifies and mechanical properties gradually weaken. In addition, by comparing the data under different confining pressures after the same freezing–thawing times, it is found that the peak deviatoric stress and elastic modulus increase gradually. The above analysis reveals that freezing–thawing cycles have damage and deterioration effect on sandstone, while confining pressure shows the ability to improve rock strength.

Damage constitutive model under the combined action of freezing–thawing and triaxial load

The damage mechanism of rock can be better revealed from the perspective of energy. For example, Ning et al. (2018) proposed the crack initiation threshold during triaxial compression of rock based on energy dissipation. Li et al. (2019) established the damage model of rock from the perspective of energy dissipation. Therefore, the principle of minimum energy dissipation was used to establish the damage constitutive equation under freezing–thawing and triaxial load in this study.
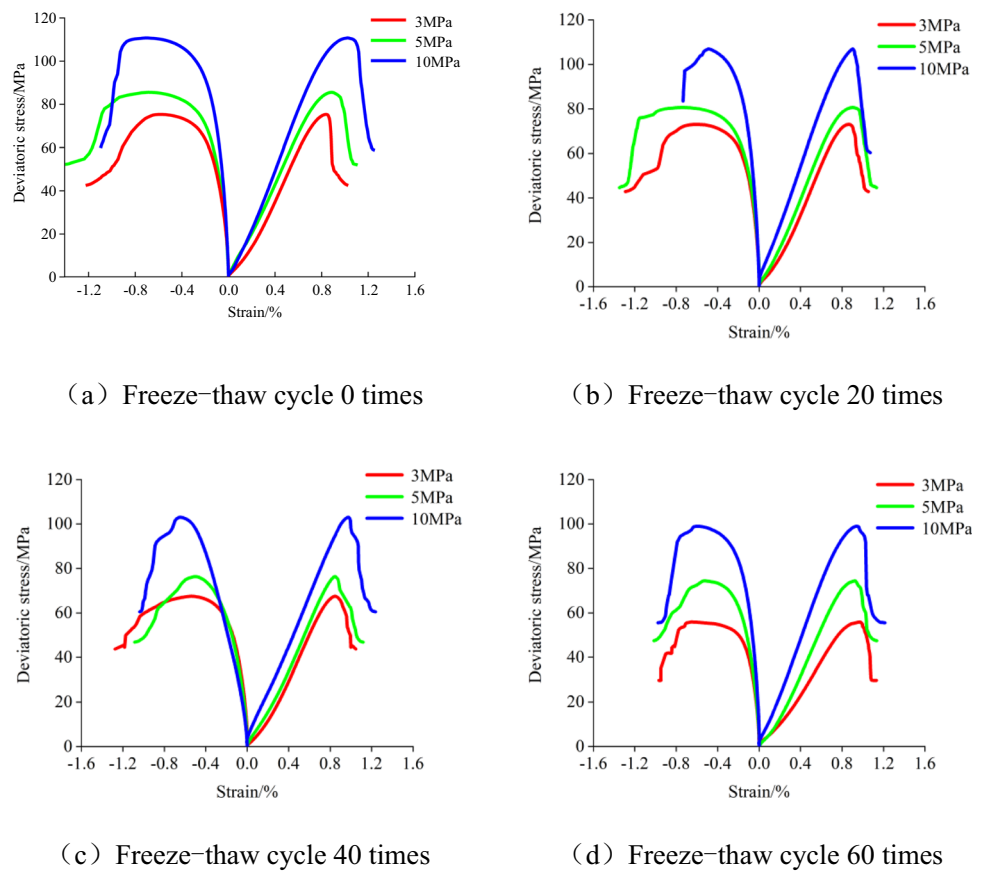
The principle of minimum energy dissipation

The principle of minimum energy dissipation is based on the principle of minimum entropy. Zhou (2001) first defined the principle of minimum energy dissipation as that each instantaneous micro-system in all energy consumption processes would be conducted in the minimum energy consumption mode under corresponding constraints. The energy dissipation rate can be expressed as

$$\varphi = TP = T \sum_{k=1}^{n} J_k X_k \tag{1}$$

where T represents the absolute temperature of the micro-system, P represents the rate of entropy, J_k represents the kth irreversible thermodynamic flow, and X_k represents the heat of the kth irreversible thermodynamic process. The relation curve between the entropy rate P and the time t can be approximated by a first-order trapezoidal line. In the approximation process, the energy dissipation rate of the micro-system is minimized, so the nonlinear nonequilibrium problem can be transformed into a linear nonequilibrium problem in a micro-time period.

Fig. 5 Stress–strain curves of triaxial compression under different freezing–thawing cycles

（a）Freeze–thaw cycle 0 times

（b）Freeze–thaw cycle 20 times

（c）Freeze–thaw cycle 40 times

（d）Freeze–thaw cycle 60 times

Table 2 Test results of peak deviatoric stress, peak deviatoric strain, and elastic modulus

Confining pressure (MPa)	Number of freeze–thaw cycles	Peak deviator stress (MPa)	Axial strain at failure (‰)	Elastic modulus (GPa)	Poisson ratio
3 MPa	0	78.21	8.42	12.00	0.21
	20	75.91	8.64	11.22	0.22
	40	70.50	8.47	10.58	0.23
	60	58.89	9.68	8.08	0.2
5 MPa	0	90.55	8.88	12.50	0.22
	20	85.62	8.97	12.20	0.25
	40	80.98	8.30	12.40	0.26
	60	79.35	9.19	10.47	0.22
10 MPa	0	120.72	10.26	13.85	0.28
	20	116.98	9.05	13.58	0.32
	40	112.97	9.73	13.31	0.35
	60	108.90	9.32	13.05	0.38

The establishment of damage constitutive model

Freeze–thaw damage process is essentially a process of energy consumption. Therefore, the process conforms to the principle of minimum energy dissipation. Assume that the principal stress acting on the rock micro-unit is σ_i ($i = 1, 2, 3$), and the unrecoverable strain $\dot{\varepsilon}_i^N(t)$ (t is the time parameter in the energy dissipation process) generated in the process of rock mass damage is regarded as the only energy dissipation system in the process of rock mass failure. Therefore, the energy dissipation rate of the unit at the beginning of failure can be expressed as

$$\varphi(t)|_{t=0} = \sigma_i \dot{\varepsilon}_i^N(t)|_{t=0} \tag{2}$$

According to Hooke's law, the constitutive model of rock is

$$\begin{cases} \varepsilon_1 = \frac{1}{E}[\sigma_1 - \mu(\sigma_2 + \sigma_3)] \\ \varepsilon_2 = \frac{1}{E}[\sigma_2 - \mu(\sigma_1 + \sigma_3)] \\ \varepsilon_3 = \frac{1}{E}[\sigma_3 - \mu(\sigma_1 + \sigma_2)] \end{cases} \tag{3}$$

where ε_1, ε_2, and ε_3 are the main strains; σ_1, σ_2, and σ_3 are the main stresses; and E and μ represent the elastic modulus and Poisson's ratio of rock, respectively.

According to the principle of strain equivalence, the strain caused by the stress is a constant value, which is independent of time t. The change of strain is caused by the damage in a micro-period, so Eq. (3) can be expressed as

$$\begin{cases} \varepsilon_1(t) = \frac{1}{[1-D(t)]E}[\sigma_1 - \mu(\sigma_2 + \sigma_3)] \\ \varepsilon_2(t) = \frac{1}{[1-D(t)]E}[\sigma_2 - \mu(\sigma_1 + \sigma_3)] \\ \varepsilon_3(t) = \frac{1}{[1-D(t)]E}[\sigma_3 - \mu(\sigma_1 + \sigma_2)] \end{cases} \tag{4}$$

where $\varepsilon_1(t)$, $\varepsilon_2(t)$, and $\varepsilon_3(t)$ represent the principal strains at time t and $D(t)$ represents the damage variable at time t.

The elastic modulus before and after the damage was used to represent the damage variable; then,

$$D(t) = 1 - \frac{E\prime(t)}{E} \tag{5}$$

where $E\prime(t)$ represents the elastic modulus after damage.

In the damage process, the energy dissipation rate is

$$\varphi(t) = \sigma_i \dot{\varepsilon}_i^N(t) \tag{6}$$

It is assumed that the strain rate caused by damage during energy consumption is equal to the unrecoverable strain rate. The unrecoverable principal strain rate can be obtained from Eq. (4) as follows:

$$\begin{cases} \dot{\varepsilon}_1^N(t) = \frac{-\dot{D}(t)}{[1-D(t)]^2 E}[\sigma_1 - \mu(\sigma_2 + \sigma_3)] \\ \dot{\varepsilon}_2^N(t) = \frac{-\dot{D}(t)}{[1-D(t)]^2 E}[\sigma_2 - \mu(\sigma_1 + \sigma_3)] \\ \dot{\varepsilon}_3^N(t) = \frac{-\dot{D}(t)}{[1-D(t)]^2 E}[\sigma_3 - \mu(\sigma_1 + \sigma_2)] \end{cases} \tag{7}$$

where $\dot{D}(t)$ represents the derivative of $D(t)$ at time t.

Substituting Eq. (7) into Eq. (6) yields

$$\varphi(t) = \frac{-\dot{D}(t)}{[1-D(t)]^2 E}[\sigma_1^2 + \sigma_2^2 + \sigma_3^2 - 2\mu(\sigma_1\sigma_2 + \sigma_3\sigma_2 + \sigma_1\sigma_3)] \tag{8}$$

When the rock is subjected to conventional triaxial compression ($\sigma_2 = \sigma_3$), the energy consumption rate can be re-expressed as

$$\varphi(t) = \frac{-\dot{D}(t)}{[1-D(t)]^2 E}[\sigma_1^2 + 2(1-\mu)\sigma_3^2 - 4\mu\sigma_1\sigma_3] \tag{9}$$

According to Mohr–Coulomb criterion, the constraint condition of rocks in the process of energy dissipation can be expressed as

$$F(\sigma_1, \sigma_3) = \sigma_1 - H\sigma_3 - S \tag{10}$$

where H and S represent the material parameters, which can be obtained by fitting σ_1 and σ_3 under different freezing–thawing cycles.

According to the principle of minimum energy dissipation, the energy dissipation rate of rocks at any time will take the extreme value under the constraint condition (Eq. (10)), which can be expressed as

$$\frac{\partial[\varphi + \lambda^* F(\sigma_1, \sigma_3)]}{\partial \sigma_i} = 0, (i = 1, 3) \tag{11}$$

where λ^* represents a Lagrange multiplier.

The strain produced by stress has nothing to do with time t. The damage evolution equation can be deduced by combining Eqs. (9), (10), and (11) as follows:

$$D = 1 - \exp[\frac{\lambda^* t(2\varepsilon_3 - H\varepsilon_1)}{8\varepsilon_1\varepsilon_3} + C_3] \tag{12}$$

where D is the damage variable and C_3 is the integral parameter, which is related to rock properties.

Considering that the elastic modulus of sandstone increases continuously at the initial compaction stage, Eq. (12) does not truly reflect the characteristics of pore compaction of sandstone under load. Therefore, the correction coefficient i is introduced to correct the damage, and the corrected expression is as follows:

$$1 - D^* = i[1 - D(t)] \tag{13}$$

where D^* represents the modified damage factor of sandstone and i represents the correction coefficient, which can be determined by the shape function of the initial compaction stage of the rock sample. It can be assumed to be a high-order parabola. Therefore, the correction coefficient is expressed as (Qu et al. 2018)

$$i = ax^{b-1} \tag{14}$$

where a represents the shape coefficient, $a > 0$, and b is a parameter related to rock properties. Therefore, the modified sandstone damage evolution equation is

$$D^* = 1 - a\varepsilon^{b-1}\exp[\frac{\lambda^* t(2\varepsilon_3 - H\varepsilon_1)}{8\varepsilon_1\varepsilon_3} + C_3] \tag{15}$$

The method of controlling the loading rate is often used in tests, and the stress–strain curve is calculated from the

force–displacement curve. Therefore, the displacement and strain in the loading process can be expressed as

$$x = vt \tag{16}$$

$$\varepsilon = \frac{\Delta h}{h} \tag{17}$$

where x represents the loading displacement, v represents the loading speed, Δh is the displacement in loading direction, and h is the height of the rock sample.

The axial compression loading rate is 0.1 mm/min and the rock sample height is 100 mm. The loading time of confining pressure is ignored, so t is

$$t = \frac{\varepsilon_1}{0.001} \tag{18}$$

Introducing parameter $\lambda_3^* = \lambda^* \frac{(2\varepsilon_3 - H\varepsilon_1)^2}{0.008\varepsilon_1\varepsilon_3}$ and substituting Eq. (18) into Eq. (15):

$$D^* = 1 - a\varepsilon_1^{b-1}\exp(\frac{\lambda_3^*\varepsilon_1}{2\varepsilon_3 - H\varepsilon_1} + C_3) \tag{19}$$

Assuming that the rock is isotropic material and the undamaged part bears all the load, the damage evolution equation of the rock only in the freezing–thawing process is

$$\sigma_i = \sigma_i\prime(1 - D_n) \tag{20}$$

where σ_i is the nominal principal stress, $\sigma_i\prime$ is the real principal stress, and D_n is the freezing–thawing damage factor.

Based on Hooke's law, the damage constitutive expression of rock under load is

$$\sigma'_i = E_0\varepsilon_i(1 - D^*) + \mu(\sigma_1 + \sigma_2 + \sigma_3 - \sigma_i); (i = 1, 2, 3) \tag{21}$$

where E_0 represents the elastic modulus of unfreezing-thawing rock.

Equation (19) was introduced into Eq. (21) to obtain the constitutive equation of rock damage under triaxial stress:

$$\sigma\prime_1 = a\varepsilon_1^b E_0\exp(\frac{\lambda_3^*\varepsilon_1}{2\varepsilon_3 - H\varepsilon_1} + C_3) + (2\mu - 1)\sigma_3 \tag{22}$$

The freezing–thawing damage factor based on dissipation energy ratio proposed by Feng et al. (2022) was introduced, namely:

$$D_n = \frac{|\lambda_N - \lambda_0|}{\lambda_0} \tag{23}$$

By substituting Eqs. (22) and (23) into Eq. (20), the damage constitutive equation under the coupling action of freezing–thawing and triaxial load is
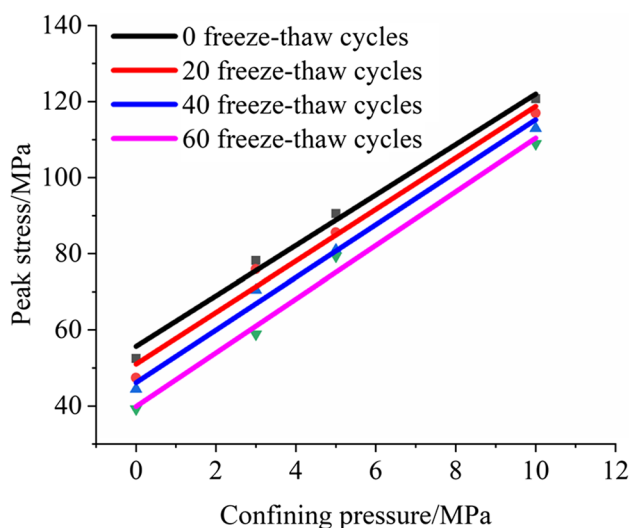
Fig. 6 Peak stress diagram of freeze–thaw sandstone under different confining pressures

$$\sigma_1 = [a\varepsilon_1^b E_0\exp(\frac{\lambda_3^*\varepsilon_1}{2\varepsilon_3 - H\varepsilon_1} + C_3) + (2\mu - 1)\sigma_3](1 - \frac{|\lambda_N - \lambda_0|}{\lambda_0}) \tag{24}$$

According to the stress–strain curve, there is the following relationship at the peak point:

$$\begin{cases} \varepsilon_1 = \varepsilon_{1c}, \sigma_1 = \sigma_{1c} \\ \varepsilon_1 = \varepsilon_{1c}, d\sigma_1/d\varepsilon_1 = 0 \end{cases} \tag{25}$$

where ε_{1c} and σ_{1c} are the peak strain and peak stress, respectively.

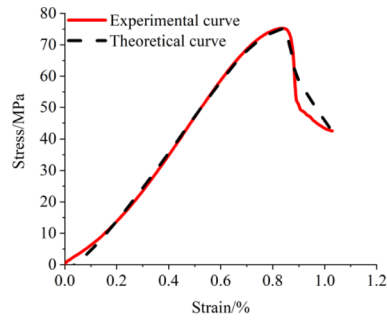Parameters λ_3^* and C_3 can be obtained by combining Eqs. (24) and (25):

$$\lambda_3^* = \frac{-b(2\varepsilon_{3c} - H\varepsilon_{1c})^2}{2\varepsilon_{1c}\varepsilon_{3c}} \tag{26}$$

$$C_3 = \ln[\frac{\sigma_{1c} - (2\mu - 1)(1 - \frac{|\lambda_N - \lambda_0|}{\lambda_0})\sigma_{3c}}{(1 - \frac{|\lambda_N - \lambda_0|}{\lambda_0})E_0 a\varepsilon_{1c}^b}] + \frac{b(2\varepsilon_{3c} - H\varepsilon_{1c})}{2\varepsilon_{3c}} \tag{27}$$
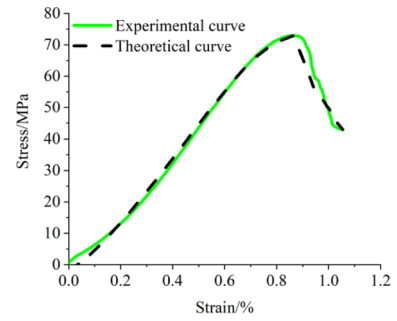
Table 3 Fitting results of parameters H and S

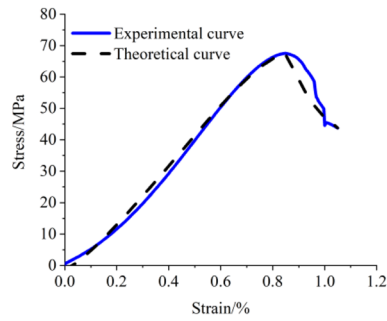| Number of freeze–thaw cycles (N)	H	S	R^2
0	6.63	55.66	0.99
20	6.77	50.99	0.98
40	6.91	46.13	0.99
60	7.05	39.85	0.99

Fig. 7 Comparison of test and constitutive model curves for frozen-thawed sandstone ($\sigma_3 = 3$ MPa)
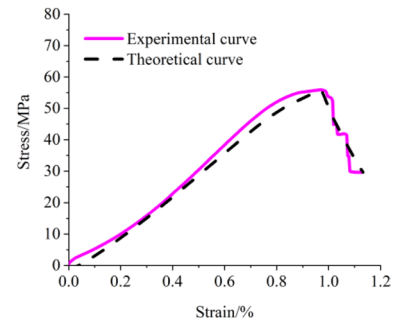

(a) Comparison of test and constitutive model curves at 0 freeze−thaw cycles

(b) Comparison of test and constitutive model curves at 20 freeze−thaw cycles
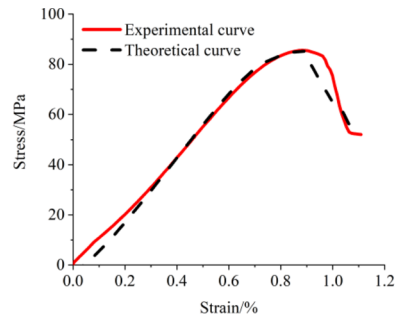
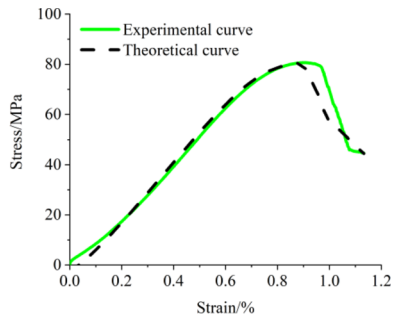(c) Comparison of test and constitutive model curves at 40 freeze−thaw cycles

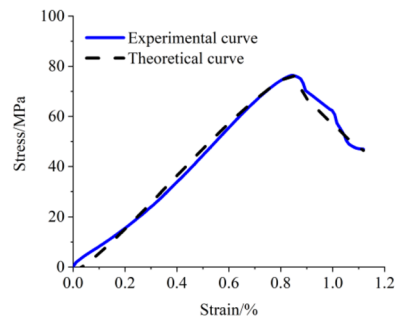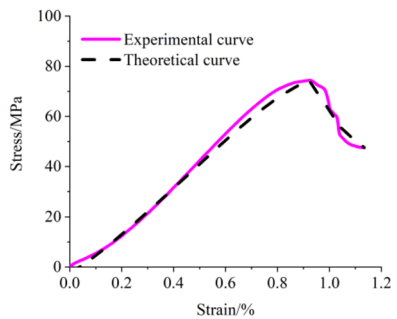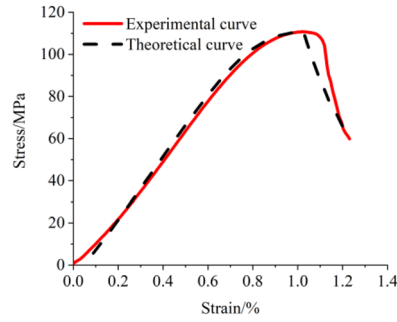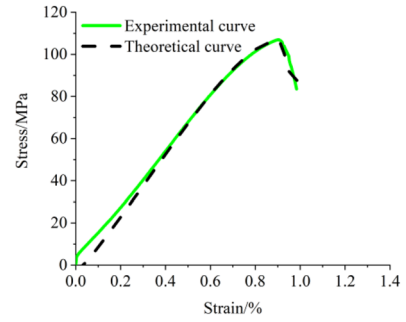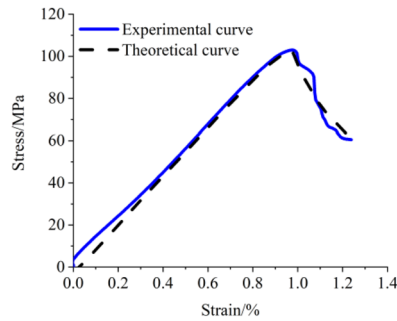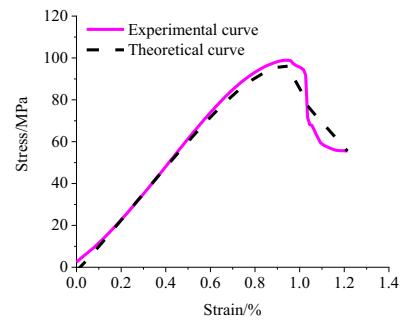(d) Comparison of test and constitutive model curves at 60 freeze−thaw cycles

Fig. 8 Comparison of test and constitutive model curves for frozen-thawed sandstone ($\sigma_3 = 5$ MPa)

(a) Comparison of test and constitutive model curves at 0 freeze−thaw cycles

(b) Comparison of test and constitutive model curves at 20 freeze−thaw cycles

(c) Comparison of test and constitutive model curves at 40 freeze−thaw cycles

(d) Comparison of test and constitutive model curves at 60 freeze−thaw cycles

Fig. 9 Comparison of test and constitutive model curves for frozen-thawed sandstone ($\sigma_3 = 10$ MPa)

(a) Comparison of test and constitutive model curves at 0 freeze−thaw cycles

(b) Comparison of test and constitutive model curves at 20 freeze−thaw cycles

(c) Comparison of test and constitutive model curves at 40 freeze−thaw cycles

(d) Comparison of test and constitutive model curves at 60 freeze−thaw cycles

Table 4 Model parameters under different freeze–thaw cycles ($\sigma_3 = 3$ MPa)

Number of freeze–thaw cycles	a_1	b	c	d	λ_3^*	C_3
0	1.0002	1.3295	1.1830	−0.2124	60.5399	0.3333
20	1.1054	1.3030	1.0258	−0.2059	61.7589	0.3858
40	1.1335	1.2653	0.7156	−0.1798	66.9698	0.4461
60	1.4933	1.2249	2.2456	−0.1461	64.3892	0.5179

Table 5 Model parameters under different freeze–thaw cycles ($\sigma_3 = 5$ MPa)

Number of freeze–thaw cycles	a_1	b	c	d	λ_3^*	C_3
0	0.9992	1.2749	0.7096	−0.3019	54.9819	−0.0803
20	1.0246	1.2546	1.0568	−0.2965	54.8735	0.0756
40	1.0423	1.2359	0.7256	−0.2293	66.7328	0.3046
60	1.1990	1.2134	0.9856	−0.1820	71.7984	0.6432

Table 6 Model parameters under different freeze–thaw cycles ($\sigma_3 = 10$ MPa)

Number of freeze–thaw cycles	a_1	b	c	d	λ_3^*	C_3
0	1.0004	1.1866	1.6296	−0.3563	55.1315	0.1460
20	1.0199	1.1526	0.5837	−0.2935	65.5805	0.4477
40	1.0637	1.1106	1.1756	−0.3118	57.0975	1.0119
60	1.0882	1.0915	1.1856	−0.2568	61.0401	2.21869

Fig. 10 The relationship between fitting parameters and freeze–thaw times ($\sigma_3 = 3$ MPa)

(a) Fitting curve of a_1

(b) Fitting curve of b

(c) Fitting curve of $d\lambda_3^*$

(b) Fitting curve of C_3
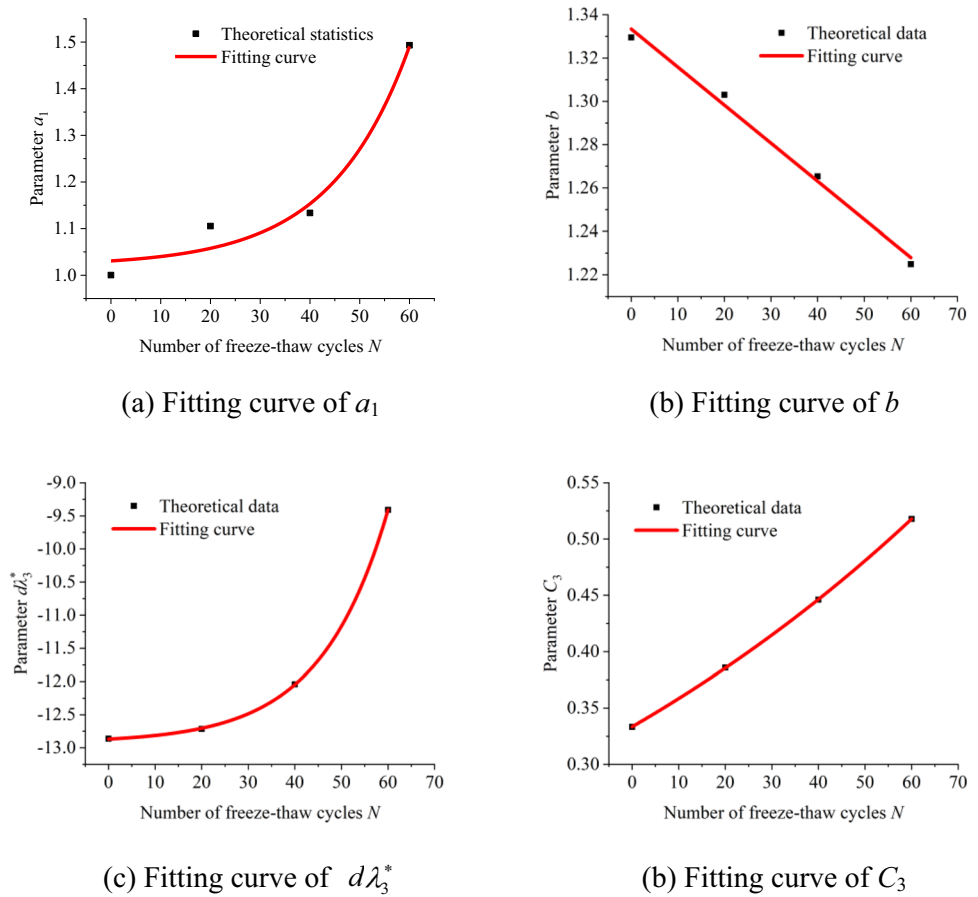
When Eqs. (26) and (27) are substituted into Eq. (24), curve shape parameter a will be eliminated in the calculation process, resulting in the failure of the correction effect of i. Therefore, the curve shape correction factor a_1 is further introduced into C_3 to ensure the correction effect of a, which causes the data in Eq. (24) to change. In order to regulate this change, a new parameter d needs to be introduced. Thus, the piecewise constitutive model finally established is as follows:

$$\sigma = \begin{cases} \left[a\varepsilon_1^b E_0 \exp\left(M_1 + M_2\right) + (2\mu - 1)\sigma_{3c}\left(1 - \frac{|\lambda_N - \lambda_0|}{\lambda_0}\right)\right], \varepsilon_1 \leq \varepsilon_{1c} \\ \left[a\left[\varepsilon_{1c} - c\left(\varepsilon_1 - \varepsilon_{1c}\right)\right]^b E_0 \exp\left(M_1 + M_2\right) + (2\mu - 1)\sigma_{3c}\right]\left(1 - \frac{|\lambda_N - \lambda_0|}{\lambda_0}\right), \varepsilon_1 > \varepsilon_{1c} \end{cases} \tag{28}$$
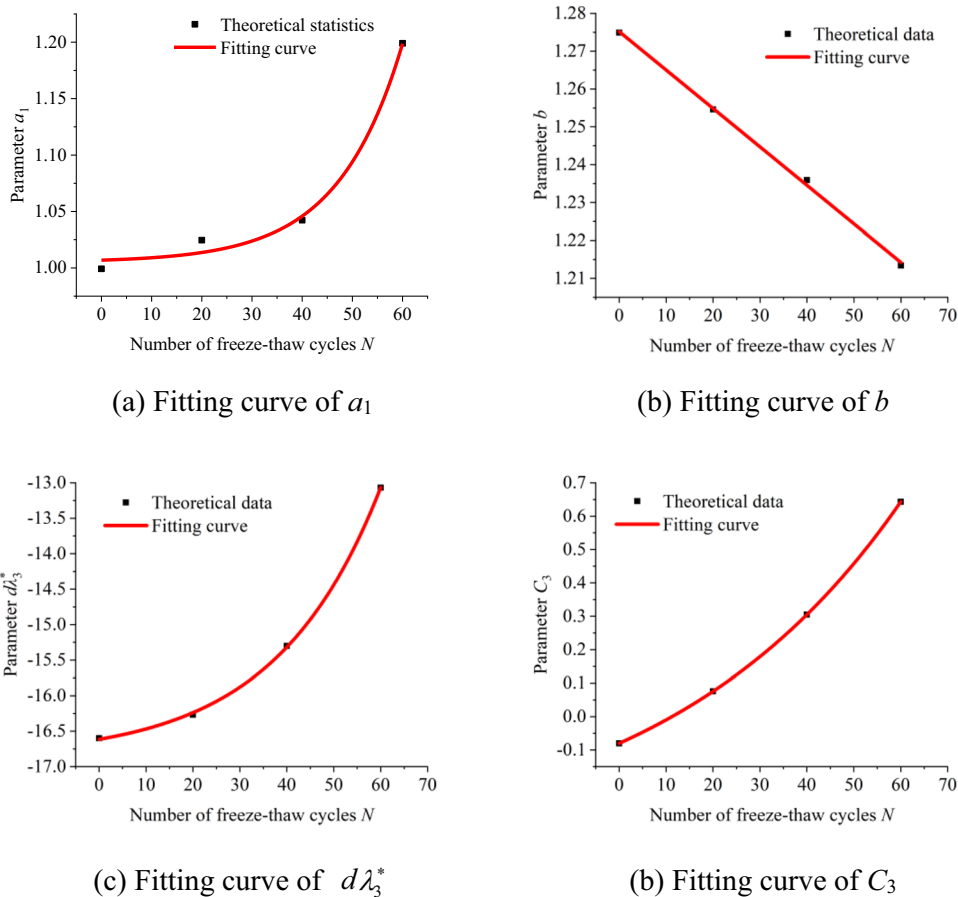
where

$$\begin{cases} M_1 = \frac{-db\varepsilon_1(2\varepsilon_{3c} - H\varepsilon_{1c})^2}{2\varepsilon_{1c}\varepsilon_{3c}(2\varepsilon_3 - H\varepsilon_1)} + \frac{db(2\varepsilon_{3c} - H\varepsilon_{1c})}{2\varepsilon_{3c}} \\ M_2 = ln\left[\frac{\sigma_{1c} - (2\mu - 1)(1 - \frac{|\lambda_N - \lambda_0|}{\lambda_0})\sigma_{3c}}{(1 - \frac{|\lambda_N - \lambda_0|}{\lambda_0})a_1 E_0 a\varepsilon_{1c}^b}\right] \end{cases} \tag{29}$$

and c is a damage characteristic value of sandstone after peak.

Model validation

Table 2 shows the peak strength of triaxial compression under different freeze–thaw cycles. The material parameters H and S can be obtained by fitting method, and the results are shown in Fig. 6 and Table 3. The results show that the ultimate strength of rock samples decreases overall, and the slope of the curve increases slightly with the number of freeze–thaw cycles.

The freeze–thaw damage factor based on the dissipation energy ratio, the material parameter H, and the related parameters (including Poisson's ratio, elastic modulus, peak deviatoric stress, axial peak strain, and radial peak strain) measured by indoor triaxial test were introduced into Eq. (28) to obtain the damage constitutive model under freezing–thawing and triaxial load. The theoretical curves of damage constitutive model under the combination of confining pressure ($\sigma_3 = 3$ MPa, 5 MPa, and 10 MPa) and freezing–thawing

Fig. 11 The relationship between fitting parameters and freeze–thaw times ($\sigma_3 = 5$ MPa)

(a) Fitting curve of a_1

(b) Fitting curve of b

(c) Fitting curve of $d\lambda_3^*$

(b) Fitting curve of C_3

cycles ($N = 0$, 20, 40, and 60) can be obtained, respectively, by fitting the test stress–strain curves, as shown in Figs. 7, 8, and 9. According to the fitting results, parameters a_1, b, c, d, λ_3^*, and C_3 were obtained, as shown in Tables 4, 5, and 6.

According to the comparison results of the above curves, it can be seen that under different confining pressures, the theoretical curve and the test curve have a high degree of coincidence in the pre-peak stage and post-peak stage. In addition, the stress–strain relationship, peak strength, and elastic modulus of the rock are consistent with the experimental results, which indicate that the constitutive model can accurately reflect the mechanical properties of the rock at high, medium, and low confining pressures. Due to the complexity of the constitutive model, there are some differences between the theoretical and experimental values of the post-peak strain softening stage. But in general, this model can describe the mechanical behavior of frozen and thawed rocks well.

Parameter and energy analysis

Parameter analysis

The parameters in Tables 4, 5, and 6 were fitted to study the variation of each parameter with the number of freeze–thaw

cycles under different confining pressures. The specific fitting relationship was shown in Figs. 10, 11, and 12, and the fitting equation was shown in Table 7.

It can be seen from Figs. 10, 11, and 12 that the parameters a_1 increase exponentially with the number of freeze–thaw cycles under three confining pressures. It governs the peak value of the curve, and the goodness of fit exceeds 0.97, indicating a strong agreement between the peak value of the model curve and experimental data. Parameter b decreases linearly with the number of freeze–thaw cycles. It controls the curve shape before the peak, and its goodness of fit is above 0.98, so the constitutive model can be well consistent with the elastic modulus of the rock before the peak. Modified λ_3^* (i.e., $d\lambda_3^*$) and C_3 increase exponentially with the number of freeze–thaw cycles. The two aforementioned variables are correlated with a_1 and b, and they are employed for the purpose of optimizing the peak value and elastic modulus of the stress–strain curve. In general, the fit goodness of four curves is good. In the post-peak stage, micro-cracks in rock continuously expand to form macro-cracks, which make the specimen unstable and failure. The disordered state of micro-crack propagation leads to poor regularity of parameter c. Therefore, no analysis was performed here.

Fig. 12 The relationship between fitting parameters and freeze–thaw times ($\sigma_3 = 10$ MPa)

(a) Fitting curve of a_1

(b) Fitting curve of b

(c) Fitting curve of $d\lambda_3^*$

(b) Fitting curve of C_3
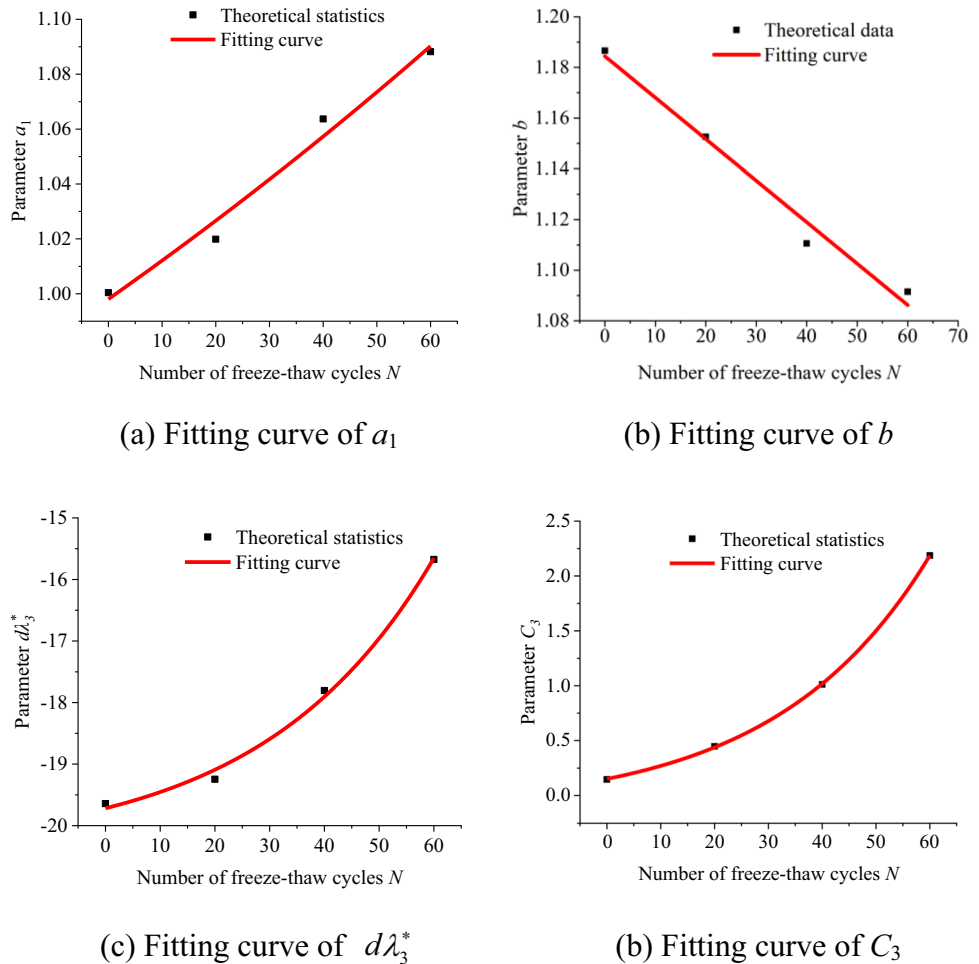
Energy analysis

According to the first law of thermodynamics, it is assumed that energy is converted only within the rock system (Xie et al. 2005). The relationship between total energy, strain energy, and dissipated energy is as follows:

$$U = U^e + U^d \tag{30}$$

where U, U^e, and U^d represent the total energy, strain energy, and dissipation energy of rock, respectively.

The total absorbed energy is

$$U = \int (\sigma_1 - 2\mu\sigma_3)d\varepsilon_1 \tag{31}$$

The elastic strain energy can be obtained by the following formula:

$$U^e = \frac{1}{2E_u}[\sigma_1^2 + 2(1 - \mu)\sigma_3^2 - 4\mu\sigma_1\sigma_3] \tag{32}$$

where E_u is the unloading modulus. According to the research of Huang et al. (2014), Wang et al. (2019), and

Xie et al. (2009), E_u can be approximately replaced by the elastic modulus E.

Taking confining pressure of 3 MPa as an example, the relationship among total energy, elastic strain energy, and

Table 7 Statistical table of parameter fitting equation

Confining pressure (MPa)	Parameter	Fitting equation	R^2
3	a_1	$a_1 = 1.02003 + 0.01065\exp(N/15.834)$	0.97
	b	$b = 1.3334 - 0.00176N$	0.98
	$d\lambda_3^*$	$d\lambda_3^* = 0.0546\exp(N/14.41) - 12.92$	0.99
	C_3	$C_3 = 0.3035\exp(N/126.40) + 0.03$	0.99
5	a_1	$a_1 = 1.00507 + 0.00181\exp(N/12.85)$	0.99
	b	$b = 1.275 - 0.00102N$	0.99
	$d\lambda_3^*$	$d\lambda_3^* = 0.2602\exp(N/22.36) - 16.87$	0.98
	C_3	$C_3 = 0.3276\exp(N/51.47) - 0.41$	1
10	a_1	$a_1 = 0.6114 + 0.3867\exp(N/280.61)$	0.98
	b	$b = 1.1844 - 0.00164N$	0.99
	$d\lambda_3^*$	$d\lambda_3^* = 0.6975\exp(N/31.24) - 20.41$	0.99
	C_3	$C_3 = 0.2832\exp(N/28.54) - 0.13$	0.99

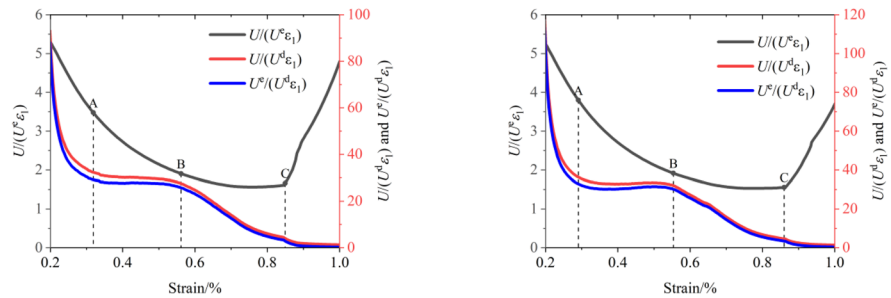**Fig. 13** Energy curves under different freeze–thaw times (σ_3 = 3 MPa)
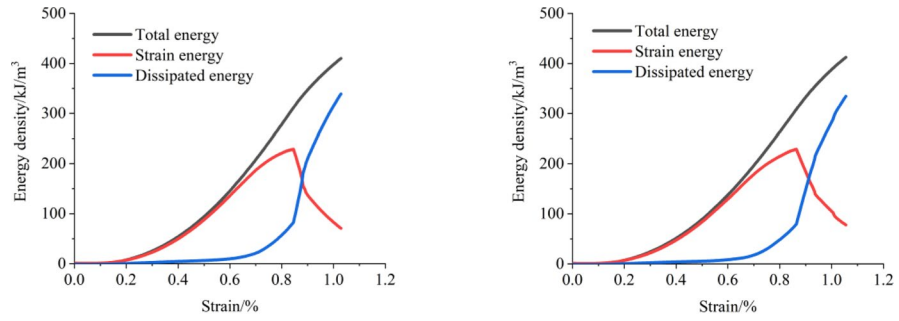
(a) Energy curve calculated by constitutive equation ($N = 0$)

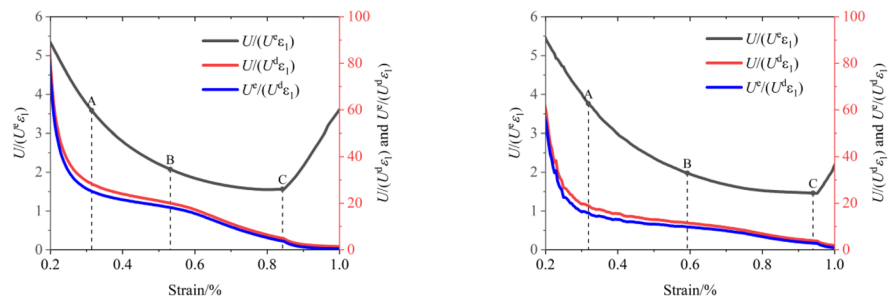(b) Energy curve calculated by constitutive equation ($N = 20$)
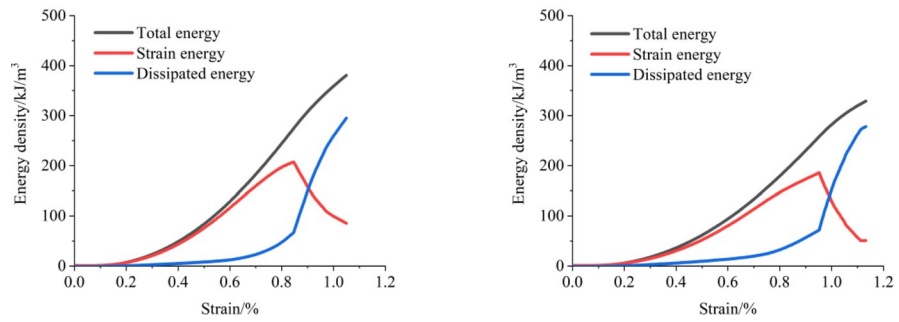
(a) Energy curve calculated by constitutive equation ($N = 40$)

(b) Energy curve calculated by constitutive equation ($N = 60$)

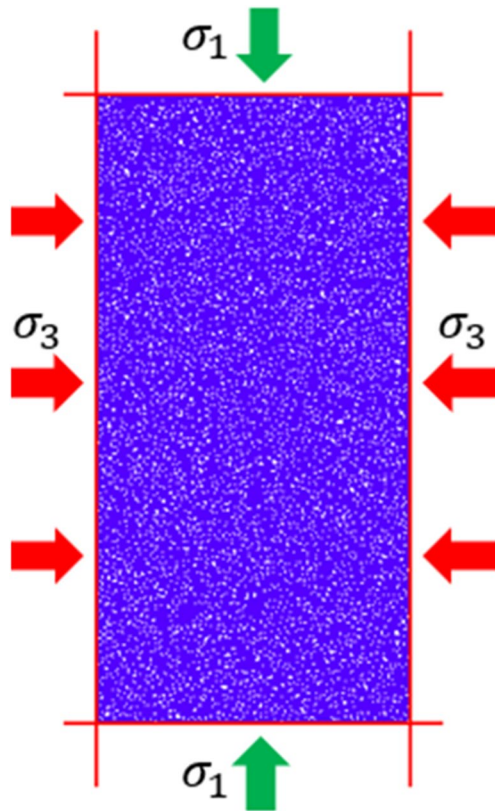**Fig. 14** Energy ratio curve of freeze–thaw sandstone (σ_3 = 3 MPa)

(a) Energy ratio curve at 0 freeze−thaw cycles

(b) Energy ratio curve at 20 freeze−thaw cycles

(c) Energy ratio curve at 40 freeze−thaw cycles

(d) Energy ratio curve at 60 freeze−thaw cycles

Table 8 Meso-mechanical parameters of the model

Confining pressure (MPa)	Particle density (kg/m³)	Stiffness ratio of particle	Parallel bond stiffness ratio	Normal strength of parallel bonding (MPa)	Shear strength of parallel bonding (MPa)	Effective modulus of particles (GPa)	Effective modulus of parallel bonding (GPa)	Coefficient of friction
3	2500	0.5	0.5	37	37	4.1	4.1	0.5
5	2500	0.8	0.8	38.5	38.5	4.9	4.9	0.5
10	2500	1.5	1.5	41.5	41.5	6.6	6.6	0.5

Fig. 15 Numerical model of triaxial compression

dissipation energy in the loading process was analyzed. The damage constitutive model (Eq. (28)) was substituted into Eqs. (31) and (32) for calculation. The relationship of total energy, elastic energy, and dissipation energy with axial strain was obtained, as shown in Fig. 13.

It can be seen from Fig. 13 that the total energy and dissipated energy increase with the increase of axial strain, while the overall trend of strain energy increases first and then decreases. This is because before the stress reaches the peak, the absorbed energy of rock is stored as strain energy. When the rock reaches and exceeds the peak, the stored strain energy is released and gradually decays to 0.

The variation law of energy ratios ($\frac{U}{U^e \varepsilon_1}$, $\frac{U}{U^d \varepsilon_1}$, and $\frac{U^e}{U^d \varepsilon_1}$) with strain was obtained (as shown in Fig. 14, where ε plays a dimensionless role).

It can be seen from Fig. 14 that $\frac{U}{U^d \varepsilon_1}$ and $\frac{U^e}{U^d \varepsilon_1}$ show a downward trend with axial strain, while $\frac{U}{U^e \varepsilon_1}$ decreases first and then increases. There are three characteristic nodes (A, B, and C) in the curve, which correspond to the four stages of rock compression. Before point A, the rock was in the compaction stage. At this stage, the energy dissipation is more, so the curves related to dissipation energy decrease sharply. Rock is in elastic stage from A to B, so the curve is relatively stable. The rock begins to be destroyed from B to C and the energy dissipation increases, so the decline rate of the curve increases compared with the elastic stage. After point C, the strain energy is gradually released to 0, so the ratio of total energy to strain energy will increase.

The value of $\frac{U}{U^e \varepsilon_1}$ at point C was 1.66, 1.56, 1.56, and 1.46 when the number of freeze–thaw cycles was 0, 20, 40, and 60, respectively. It indicates that the precursor information value of damage gradually decreases with the freeze–thaw cycle. When the freeze–thaw cycles were 0, 20, 40, and 60, the strain spacings from B to C were 0.29, 0.31, 0.31, and 0.35, respectively, showing a gradually increasing trend. This is because the freeze–thaw cycle leads to the repeated action of frost heave force, which makes the pore of the rock sample fully developed. Thus, the brittleness of the rock decreases and the plasticity increases. The slopes at the post-point C were 20.64, 15.15, 12.97, and 12.57, respectively, showing a decreasing trend with the number of freeze–thaw cycles. The larger the slope of this stage is, the more severe the damage is. Therefore, it can be seen that the freezing–thawing action weakens the brittleness degree of rock failure.

Micro-damage and failure characteristics of rock under combined action of freezing–thawing and load
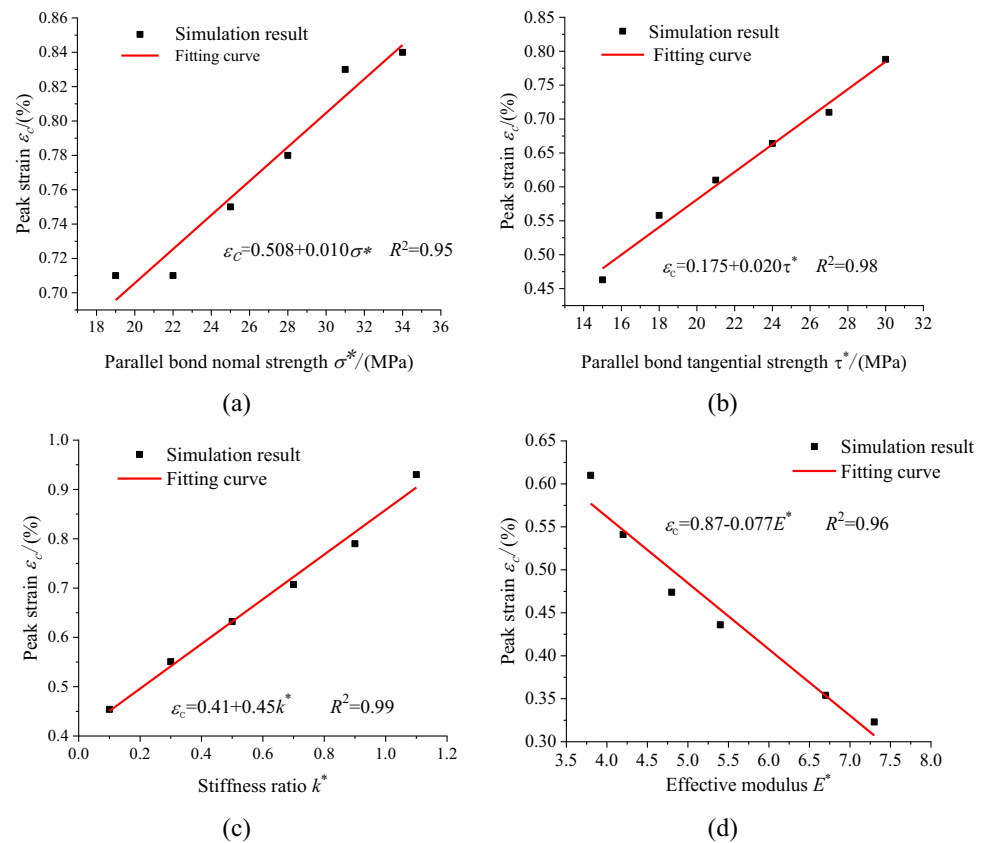
Digital specimen

PFC^{2D} was used for numerical simulation. The specimen size ratio for simulation and test is 1:1. Table 8 shows the

**Fig. 16** Influence of each parameter on peak stress

(a)

(b)

(c)

(d)
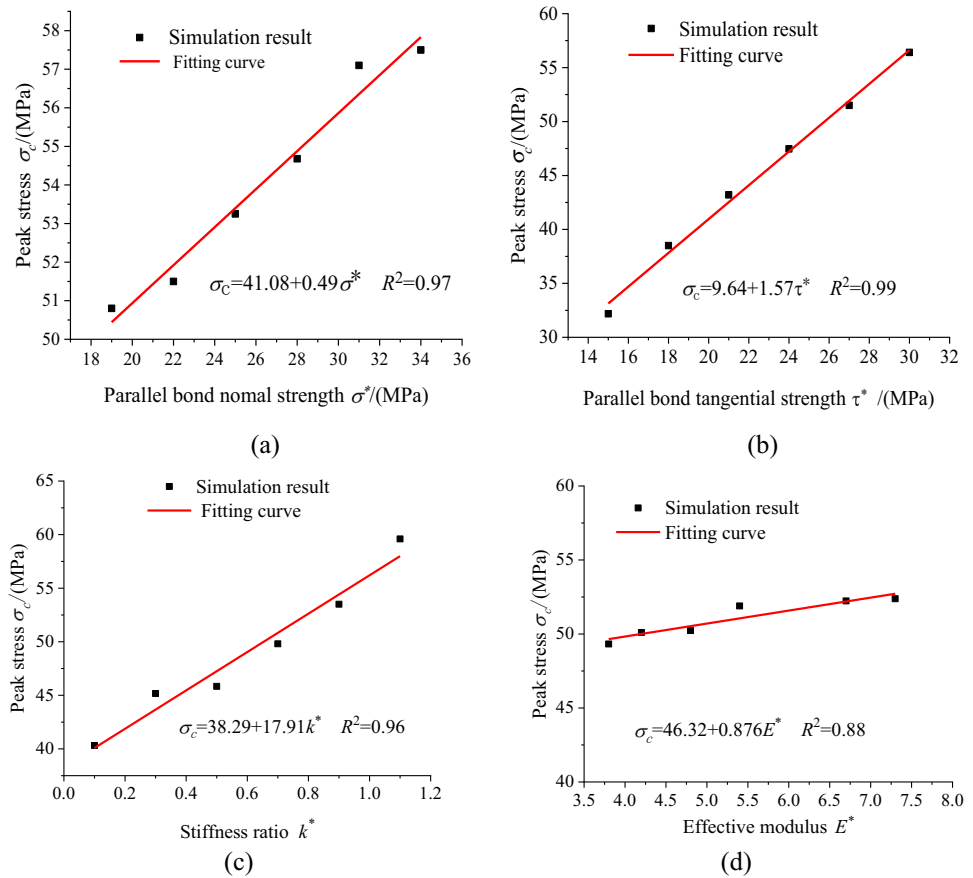
Fig. 17 Influence of each parameter on peak strain


(a)

(b)

(c)

(d)

Table 9 Mesoscopic parameters of freeze–thaw sandstone

Confining pressure (MPa)	Number of freeze–thaw cycles	Normal strength of parallel bonding (MPa)	Shear strength of parallel bonding (MPa)	Stiffness ratio	Effective modulus
3	0	37	37	0.5	4.1
	20	31.5	31.5	0.8	4.1
	40	27.5	27.5	1.1	4.1
	60	22	22	4.6	4.1
5	0	38.5	38.5	0.8	4.9
	20	32	32	1.29	4.9
	40	29	29	1.8	4.9
	60	28	28	2.55	4.9
10	0	41.5	41.5	1.5	6.6
	20	37	37	1.6	6.6
	40	35	35	1.8	6.6
	60	34	34	2.15	6.6

Fig. 18 Comparison of numerical simulation curve and experimental curve ($\sigma_3 = 3$ MPa)
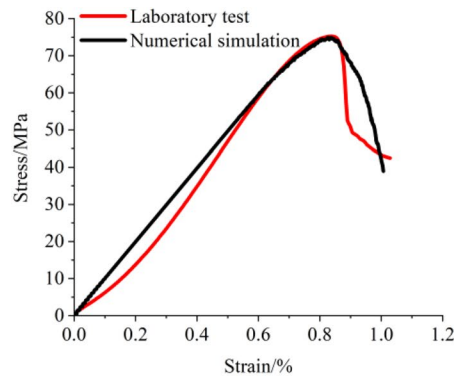
(a) 0 freeze–thaw cycles
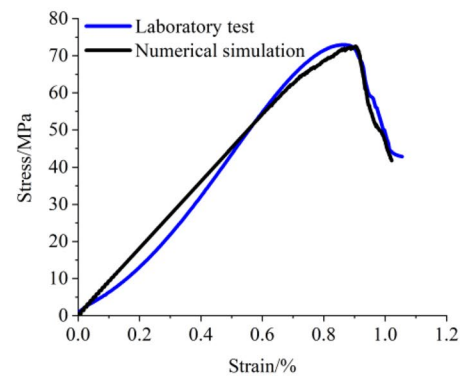
(b) 20 freeze–thaw cycles
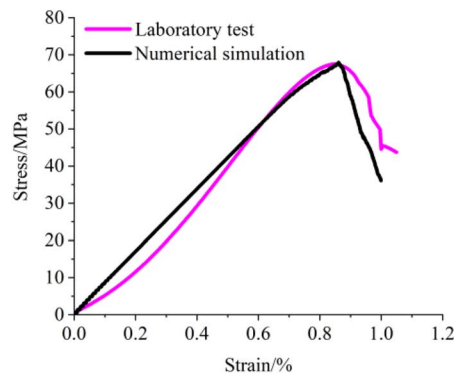
(c) 40 freeze–thaw cycles
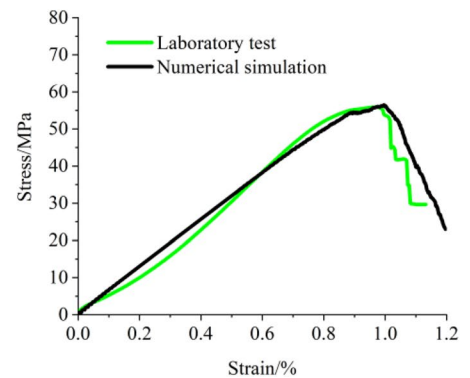
(d) 60 freeze–thaw cycles

Fig. 19 Comparison of numerical simulation curve and experimental curve ($\sigma_3 = 5$ MPa)

(a) 0 freeze−thaw cycles

(b) 20 freeze−thaw cycles

(c) 40 freeze−thaw cycles

(d) 60 freeze−thaw cycles
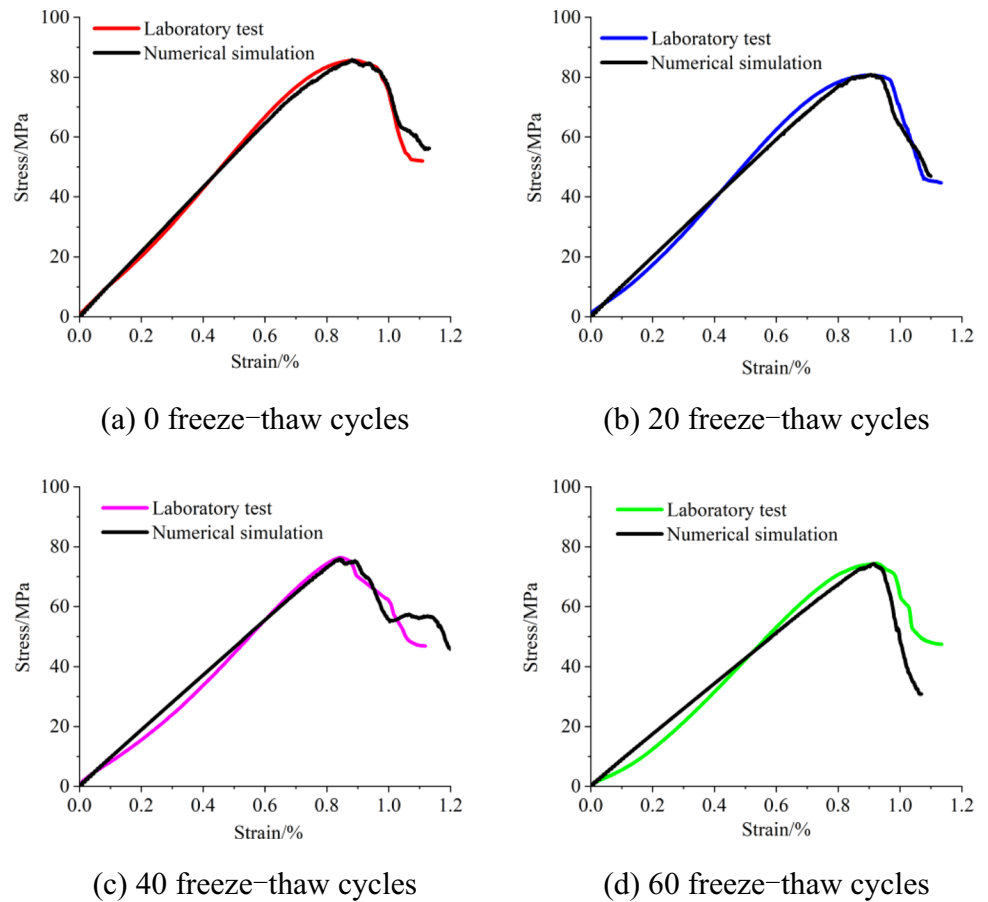
mesoscopic parameters of unfreezed-thawed rock under confining pressures of 3 MPa, 5 MPa, and 10 MPa. The sample model is shown in Fig. 15.

Determination of model parameters and comparison of results

(1) Parameter sensitivity analysis of numerical model

According to the previous research results (Feng et al. 2022), the micro-parameters that need to be adjusted in the PFC numerical model are mainly parallel bond normal strength, parallel bond tangential strength, stiffness ratio, and effective modulus. The impact of these four parameters on the peak stress is illustrated in Fig. 16, while their influence on the peak strain is depicted in Fig. 17. Based on the slope of the fitted curve, it can be seen that the degree of influence on the peak stress is in the order from large to small: stiffness ratio > parallel bond tangential strength > effective modulus > parallel bond normal strength. The order of the degree of influence on the peak strain from large to small is stiffness ratio > effective modulus > parallel bond tangential strength > parallel bond normal strength.

(2) Determination of model parameters

The meso-parameters of the model under different freezing–thawing times when the confining pressures were 3 MPa, 5 MPa, and 10 MPa were determined through multiple numerical calculations, as shown in Table 9.

(3) Comparison between test results and simulation results

Figures 18, 19, and 20 show the comparison of test curves and simulation curves under different confining pressures. It can be seen that the two groups of curves are in good agreement, indicating that the selected parameters are highly reliable.

Microscopic failure characteristic analysis

Energy analysis

The results in the literature (Feng et al. 2022) show that the accuracy of the damage model based on dissipative energy ratio is high. Therefore, this numerical simulation method is used for energy analysis. In the PFC model, the boundary energy is the work done by the loading plate on the sample.

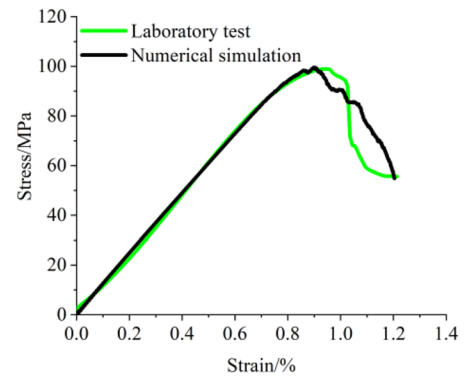**Fig. 20** Comparison of numerical simulation curve and experimental curve ($\sigma_3 = 10$ MPa)
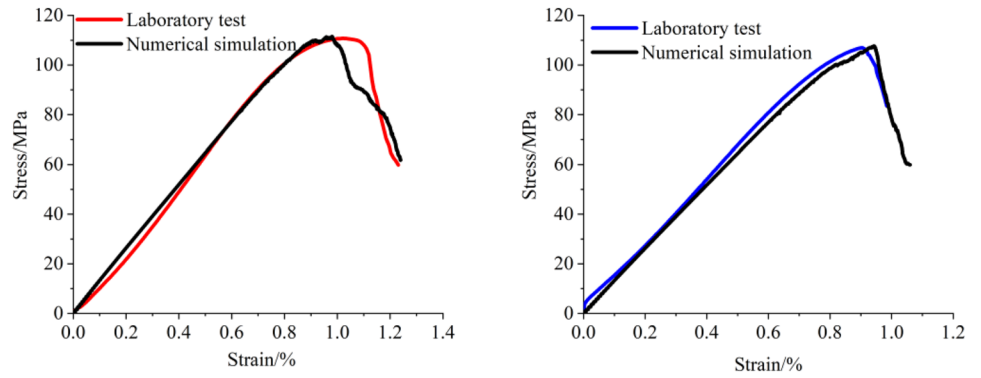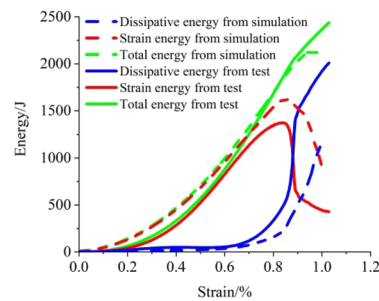
(a) 0 freeze−thaw cycles
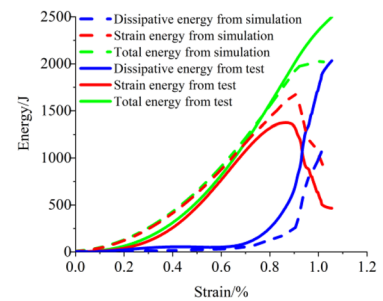
(b) 20 freeze−thaw cycles
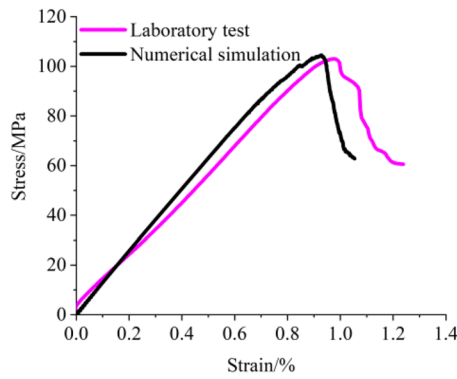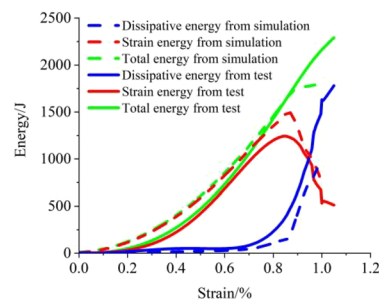
(c) 40 freeze−thaw cycles

(d) 60 freeze−thaw cycles

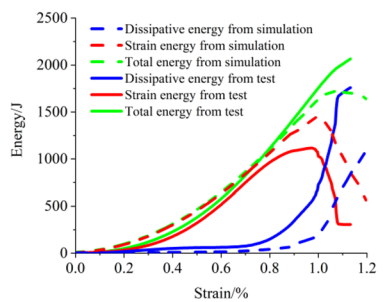**Fig. 21** Energy comparison diagram of experiment and simulation ($\sigma_3 = 3$ MPa)

(a) Energy evolution of 0 freeze−thaw cycles
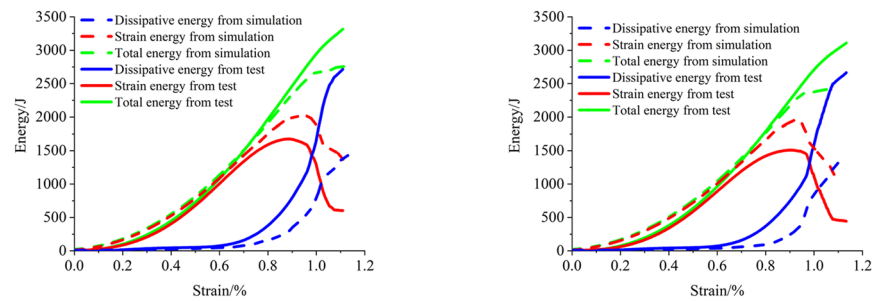
(b) Energy evolution of 20 freeze−thaw cycles
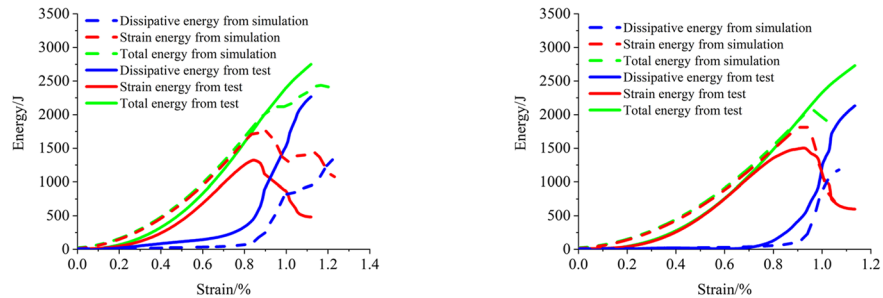
(c) Energy evolution of 40 freeze−thaw cycles

(d) Energy evolution of 60 freeze−thaw cycles

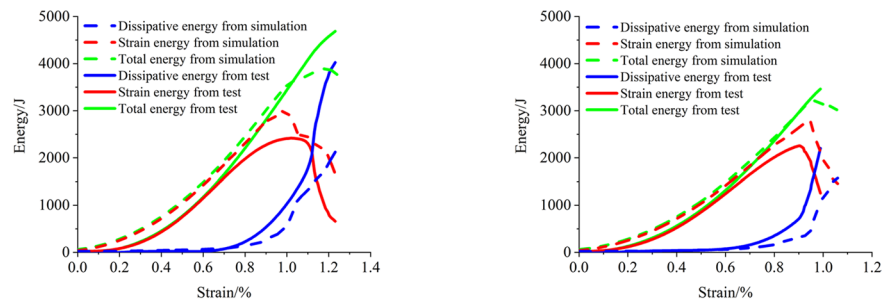**Fig. 22** Energy comparison diagram of experiment and simulation ($\sigma_3 = 5$ MPa)

(a) Energy evolution of 0 freeze−thaw cycles   (b) Energy evolution of 20 freeze−thaw cycles
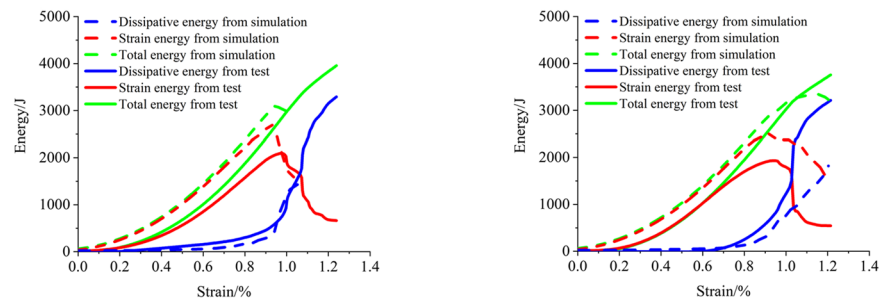
(c) Energy evolution of 40 freeze−thaw cycles   (d) Energy evolution of 60 freeze−thaw cycles

Fig. 23 Energy comparison diagram of experiment and simulation ($\sigma_3 = 10$ MPa)

(a) Energy evolution of 0 freeze−thaw cycles   (b) Energy evolution of 20 freeze−thaw cycles

(c) Energy evolution of 40 freeze−thaw cycles   (d) Energy evolution of 60 freeze−thaw cycles

The dissipated energy consists of local damping dissipated energy, kinetic energy, and sliding friction energy of particles. The total strain energy is composed of parallel bond strain energy and particle bond strain energy. The comparison of energy results between the experimental method and the numerical simulation method was shown in Figs. 21, 22, and 23.

It can be seen from the comparison results that the development trends of total energy, strain energy, and dissipation energy are consistent. Numerical calculation cannot simulate

Table 10 Statistical table of energy index at peak

Confining pressure (MPa)	Number of freeze–thaw cycles	Total energy (J)	Strain energy (J)	Dissipated energy (J)
3	0	1840	1614.08	225.92
	20	1796	1601.56	194.44
	40	1660	1505.67	154.33
	60	1581	1420.48	160.62
5	0	2283	1992.12	290.88
	20	2234	1949.27	294.73
	40	1993	1782.26	210.74
	60	1952	1820.79	131.21
10	0	3340	2936.26	403.74
	20	3184	2797.67	386.33
	40	3040	2694.51	345.49
	60	2807	2513.66	293.34

the process of pore compaction and primary crack closure at the initial stage of the test, resulting in a slight deviation between the two results. Overall, the established numerical simulation method can well simulate the mechanical behavior of freezing–thawing rock under triaxial compression.

After 0, 20, 40, and 60 freeze–thaw cycles, the corresponding energy values of peak points at confining pressures of 3 MPa, 5 MPa, and 10 MPa were shown in Table 10.

It can be seen from Table 10 that the total energy, strain energy, and dissipation energy at peak values under different confining pressures gradually decrease with the number of freezing–thawing cycles, and increase with the confining pressure under the same number of freezing–thawing cycles, indicating that the freeze–thaw action deteriorates rock and promotes its failure, while confining pressure can inhibit rock failure.

Crack propagation analysis

In the numerical simulation of specimen compression, the process of crack initiation, gradual failure, and complete connection was shown in Fig. 24.

In the figure, black area represents tensile crack and blue area represents shear crack. It can be seen that tensile cracks account for most of the number. The formation of micro-cracks is absent in the initial stage, and nearly all the energy input from external load work is transformed into elastic strain energy, as shown in Fig. 24(a). When the stress reached the crack initiation strain point, the bond strength between particles was less than the shear or tensile stress, so the bond fracture occurred and the micro-cracks appeared disorderly distribution, as shown in Fig. 24(b). As the load gradually increases, the distribution of micro-cracks gradually became regular, as shown in Fig. 24(c). This stage corresponds to the vicinity of the peak point. When the load continued to be applied, the micro-cracks converged into main cracks and shear distribution bands appeared. When the shear distribution band increased to a certain amount, the crack penetrated, resulting in the failure of the specimen, as shown in Fig. 24(d). The results of rock sample failure caused by experimental loading (Fig. 24(e)) are compared with those of numerical simulation (Fig. 24(d)), and it is found that the failure patterns of the two results are in good agreement.

The number of cracks was counted, as shown in Table 11. The growth law of crack number with strain was shown in Figs. 25, 26, and 27.

It can be seen from Table 11 that with the increase of freeze–thaw cycles, the number of shear cracks increases as a whole and is greater than the number of tensile cracks, so the tension-shear ratio is less than 1. This indicates that shear failure mainly occurs under triaxial stress.
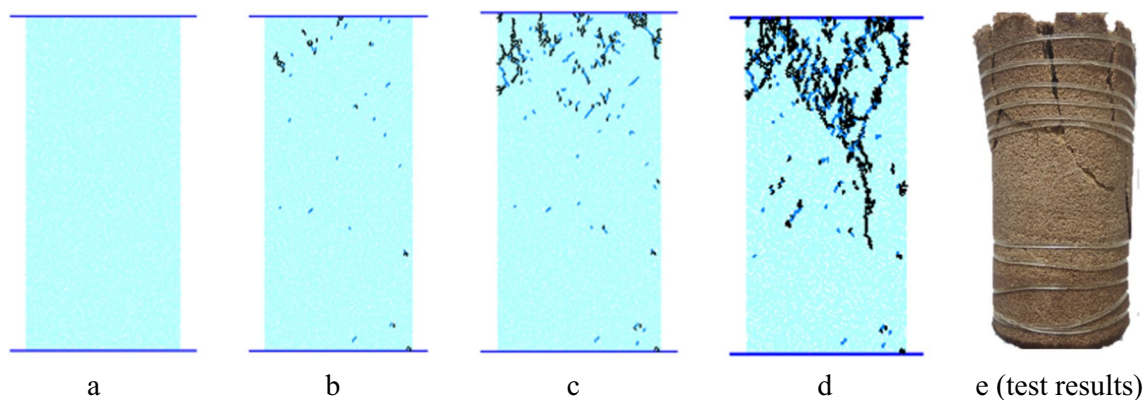
a   b   c   d   e (test results)

Fig. 24 Comparison between numerical simulation results and test results

**Table 11** Micro-crack statistics of freezing–thawing sandstone

Confining pressure (MPa)	Number of freeze–thaw cycles	Total number of cracks	Number of tensile cracks	Number of shear cracks	Tension-shear ratio
3	0	1740	747	993	0.75
	20	1895	684	1211	0.56
	40	1911	581	1330	0.44
	60	2576	198	2378	0.08
5	0	2052	717	1335	0.54
	20	1920	323	1397	0.23
	40	2122	463	1659	0.28
	60	1624	280	1344	0.21
10	0	2351	597	1654	0.36
	20	2167	607	1560	0.39
	40	2156	564	1601	0.35
	60	2871	632	2239	0.28

When the confining pressure is 3 MPa, the tension-shear ratio decreases by 25.33%, 21.43%, and 81.81% for every 20 cycles. When the confining pressures are 5 MPa and 10 MPa, respectively, the tensile-shear ratio also shows a decreasing trend. It indicates that freeze–thaw cycles promote triaxial shear failure. According to the mesoscopic evolution characteristics of crack, the failure mode of freeze–thaw rock and the role of freeze–thaw cycles can be clarified, which lays a foundation for revealing the failure mechanism of rock.

It can be seen from Figs. 25, 26, and 27 that the crack development is mainly divided into three stages. Before point D, the rock is in the elastic stage and no crack occurs. DE stage is hardening stage and cracks begin to develop. EF stage is the post-peak stage, and the cracks develop rapidly until the rock is fractured.
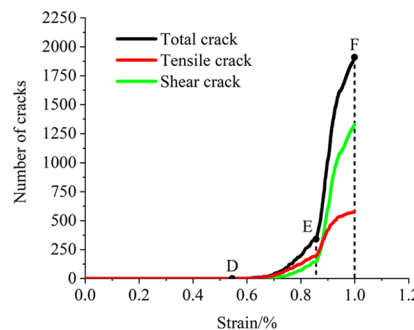
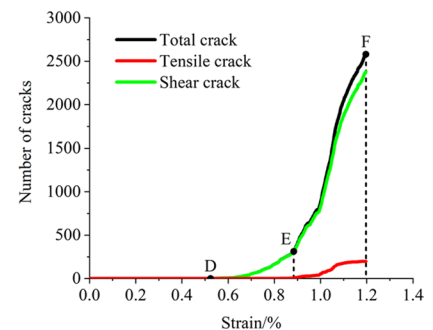**Fig. 25** Growth diagram of micro-cracks under different freeze–thaw times ($\sigma_3 = 3$ MPa)
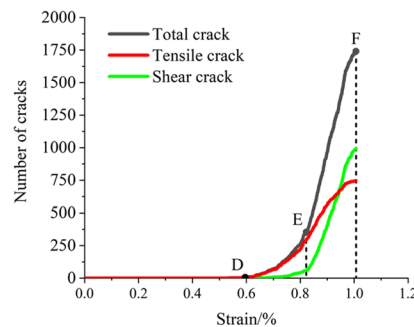
(a) Microcrack growth diagram at 0 freeze−thaw cycles
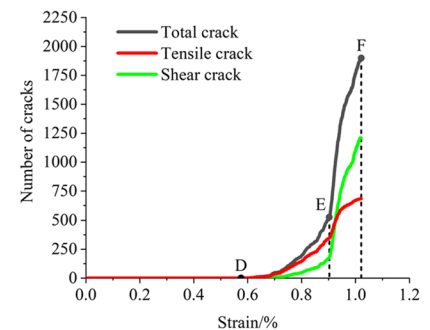
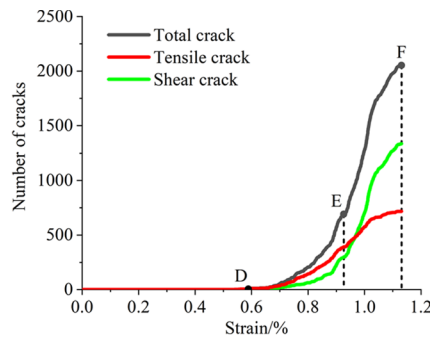(b) Microcrack growth diagram at 20 freeze−thaw cycles
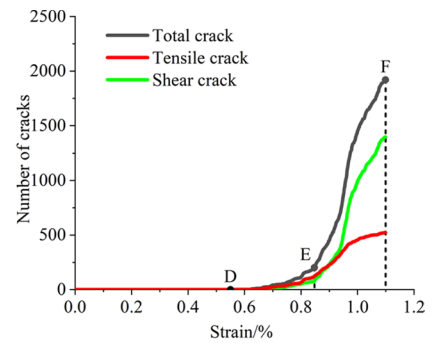
(c) Microcrack growth diagram at 40 freeze−thaw cycles
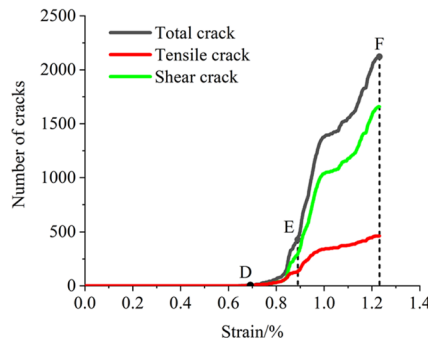
(d) Microcrack growth diagram at 60 freeze−thaw cycles

Fig. 26 Growth diagram of micro-cracks under different freeze–thaw times ($\sigma_3 = 5$ MPa)
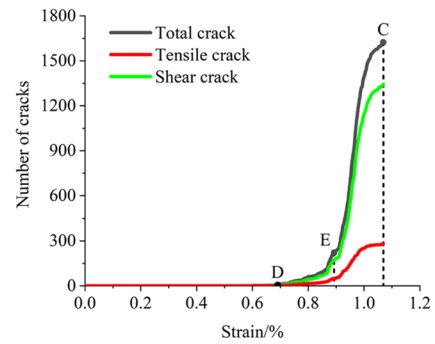

(a) Microcrack growth diagram at 0 freeze–thaw cycles

(b) Microcrack growth diagram at 20 freeze–thaw cycles

(c) Microcrack growth diagram at 40 freeze–thaw cycles

(d) Microcrack growth diagram at 60 freeze–thaw cycles

Table 12 shows the strain at crack initiation point under different freeze–thaw cycle and confining pressure.

Under the same confining pressure, the strain value corresponding to crack initiation point D shows a decreasing trend with the increase of freeze–thaw times, indicating that freeze–thaw can shorten the elastic stage of rock. With the same number of freezing–thawing times, the strain at crack initiation point D shows an overall trend of increasing as the confining pressure increases, indicating that the confining pressure can lengthen the elastic stage of rock.

Conclusion

In this paper, the triaxial damage constitutive model based on the principle of minimum energy dissipation and the dissipation energy ratio was established. The mesoscopic failure characteristics of rock during triaxial compression were studied based on PFC numerical simulation. The specific conclusions were summarized as follows:

(1) Triaxial compression test results show that the peak deviational stress of freeze–thaw rock presents a downward trend under confining pressures of 3 MPa, 5 MPa, and 10 MPa. When the confining pressure is 3 MPa, it decreases by 2.94%, 7.13%, and 16.47% for every 20 freeze–thaw cycles, respectively. When the confining pressure is 5 MPa, it decreases by 5.44%, 5.42%, and 2.01% for every 20 freeze–thaw cycles, respectively. When the confining pressure is 10 MPa, it decreases by 3.10%, 3.43%, and 3.60% for every 20 freeze–thaw cycles, respectively.

(2) Based on the Mohr–Coulomb criterion and the principle of minimum energy dissipation, the damage constitutive model under the combined action of freezing–thawing and triaxial load was obtained. The comparison between the theoretical model and triaxial compression test results shows that the model can reasonably reflect the pre-peak and post-peak mechanical properties of rock. It can provide a theoretical basis for exploring the evolution process of rock mass damage in cold regions.

(3) Based on the coupled damage constitutive model induced by freeze–thaw and triaxial loading, parameter identification and energy evolution analysis were carried out. It is found that the change of energy ratio can be divided into four stages, which correspond to
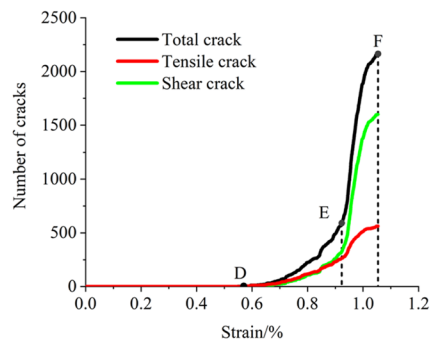
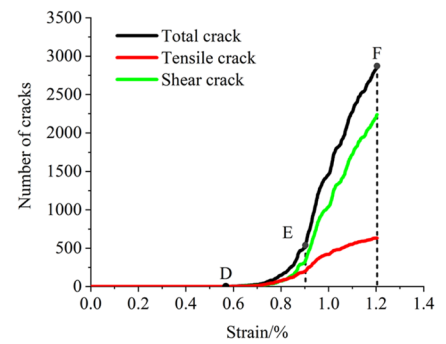**Fig. 27** Growth diagram of micro-cracks under different freeze–thaw times ($\sigma_3 =$ 10 MPa)
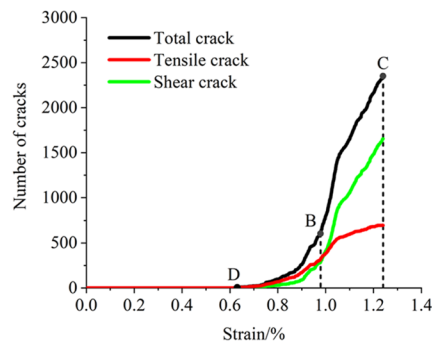
(a) Microcrack growth diagram at 0 freeze−thaw cycles
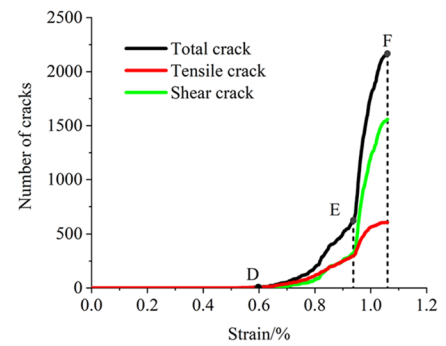
(b) Microcrack growth diagram at 20 freeze−thaw cycles

(c) Microcrack growth diagram at 40 freeze−thaw cycles

(d) Microcrack growth diagram at 60 freeze−thaw cycles

Table 12 Strain of crack initiation point under different conditions

Confining pressure (MPa)	Number of freeze–thaw cycles			
	0	20	40	60
3	0.582	0.572	0.549	0.522
5	0.596	0.569	0.554	0.599
10	0.626	0.597	0.570	0.568

the four stages of rock stress–strain curve. According to the slope analysis of the energy ratio curve after the peak, the freeze–thaw action weakened the brittleness degree of rock failure.

(4) PFC was used to establish a numerical simulation method for triaxial compression of frozen-thawed rock, and the simulated stress–strain curve was compared with the experimental results to verify the reliability of the numerical simulation method. Based on this method, it is found that the three energy indexes decrease with the number of freezing–thawing, but increase with the confining pressure. The above results show that freeze–thaw cycle promotes rock failure, while confining pressure inhibits rock failure.

(5) The crack evolution process of rock in the triaxial compression process was analyzed, which can be divided into three stages: crack-free stage, crack initiation stage, and crack rapid development stage. Under different conditions, the strain at the crack initiation point decreases with the number of freeze–thaw cycles and increases with the confining pressure, which shows that the freeze–thaw cycle reduces the elastic stage of rock, and the confining pressure increases this stage. The number of tensile and shear fractures in rock failure has been counted. It is found that the tensile-shear ratio is less than 1 and decreases with the number of freeze–thaw cycles, indicating that freeze–thaw can promote the shear failure of rock under triaxial loading.

(Disaster prevention and control team of underground engineering involved in sea).

Declarations

Conflict of interest The authors declare no competing interests.

References

Chen W, Konietzky H, Tan X, Frühwirt T (2016) Pre-failure damage analysis for brittle rocks under triaxial compression. Comput Geotech 74:45–55. https://doi.org/10.1016/j.compgeo.2015.11.018

Chen Z, He C, Ma G, Xu G, Ma C (2019) Energy damage evolution mechanism of rock and its application to brittleness evaluation. Rock Mech Rock Eng 52(4):1265–1274. https://doi.org/10.1007/s00603-018-1681-0

Feng Q, Jin J, Zhang S, Liu W, Yang X, Li W (2022) Study on a damage model and uniaxial compression simulation method of frozen-thawed rock. Rock Mech Rock Eng 55(1):187–211. https://doi.org/10.1007/s00603-021-02645-2

Guo T and Du Z (2021) Meso-numerical simulation of rock triaxial compression based on the damage model. In: Proceedings of the 3rd International Conference on Environmental Prevention and Pollution Control Technologies, Zhuhai, China, 687(1): 012134. (in Chinese)

Huang D, Li Y (2014) Conversion of strain energy in triaxial unloading tests on marble. Int J Min Sci Technol 66:160–168. https://doi.org/10.1016/j.ijrmms.2013.12.001

Krajcinovic D, Silva MAG (1982) Statistical aspects of the continuous damage theory. Int J Solids Struct 18(7):551–562. https://doi.org/10.1016/0020-7683(82)90039-7

Krautblatter M, Funk D, Günzel FK (2013) Why permafrost rocks become unstable: a rock-ice-mechanical model in time and space. Earth Surf Process Landf 38(8):876–887. https://doi.org/10.1002/esp.3374

Li T, Pei X, Wang D, Huang R, Tang H (2019) Nonlinear behavior and damage model for fractured rock under cyclic loading based on energy dissipation principle. Eng Fract Mech 206:330–341. https://doi.org/10.1016/j.engfracmech.2018.12.010

Liu XS, Ning JG, Tan YL, Gu QH (2016) Damage constitutive model based on energy dissipation for intact rock subjected to cyclic loading. Int J Rock Mech Min Sci 85:27–32. https://doi.org/10.1016/j.ijrmms.2016.03.003

Luo X, Jiang N, Fan X, Mei N, Luo H (2015) Effects of freeze-thaw on the determination and application of parameters of slope rock mass in cold regions. Cold Reg Sci Technol 110:32–37. https://doi.org/10.1016/j.coldregions.2014.11.002

Meng Q, Zhang M, Zhang Z, Han L, Pu H (2019) Research on non-linear characteristics of rock energy evolution under uniaxial cyclic loading and unloading conditions. Environ Earth Sci 78(23):1–20. https://doi.org/10.1007/s12665-019-8638-9

Ning J, Wang J, Jiang J, Hu S, Jiang L, Liu X (2018) Estimation of crack initiation and propagation thresholds of confined brittle coal specimens based on energy dissipation theory. Rock Mech Rock Eng 51(1):119–134. https://doi.org/10.1007/s00603-017-1317-9

Pan Y, Zhao Z, He L, Wu G (2020) A nonlinear statistical damage constitutive model for porous rocks. Adv Civ Eng 2020:8851914. https://doi.org/10.1155/2020/8851914

Pudasaini SP, Krautblatter M (2014) A two-phase mechanical model for rock-ice avalanches. J Geophys Res Earth Surf 119(10):2272–2290. https://doi.org/10.1002/2014JF003183

Qiu WL, Teng F, Pan SS (2020) Damage constitutive model of concrete under repeated load after seawater freeze-thaw cycles. J Constr Build Mater 236:117560. https://doi.org/10.1016/j.conbuildmat.2019.117560

Qu D, Li D, Li X, Luo Y, Xu K (2018) Damage evolution mechanism and constitutive model of freeze-thaw yellow sandstone in acidic environment. Cold Reg Sci Technol 155:174–183. https://doi.org/10.1016/j.coldregions.2018.07.012

Rakhimzhanova AK, Thornton C, Minh NH, Fok SC, Zhao Y (2019) Numerical simulations of triaxial compression tests of cemented sandstone. Comput Geotech 113:103068. https://doi.org/10.1016/j.compgeo.2019.04.013

Tian ZY, Wang W, Li XH, Xu WY (2014) A statistical damage constitutive model for brittle rocks based on the Lade-Duncan failure criterion. Adv Mater Res 919:632–636. https://doi.org/10.4028/www.scientific.net/AMR.919-921.632

Wang Z, Li Y, Wang JG (2007) A damage-softening statistical constitutive model considering rock residual strength. Comput Geosci 33(1):1–9. https://doi.org/10.1016/j.cageo.2006.02.011

Wang Y, Tan WH, Liu DQ, Hou ZQ, Li CH (2019) On anisotropic fracture evolution and energy mechanism during marble failure under uniaxial deformation. Rock Mech Rock Eng 52(10):3567–3583. https://doi.org/10.1007/s00603-019-01829-1

Wang J G, Anand S, Ye F J (2008) A statistical damage constitutive model of brittle rocks based on Weibull distribution. In: Proceedings of the first southern hemisphere international rock mechanics Symposium, Perth, Australia, pp 121–134. https://doi.org/10.36487/ACG_repo/808_167

Wen T, Liu Y, Yang C, Yi X (2018) A rock damage constitutive model and damage energy dissipation rate analysis for characterising the crack closure effect. Geomech Geoengin Int J 13(1):54–63. https://doi.org/10.1080/17486025.2017.1330969

Xie HP, Ju Y, Li LY (2005) Criteria for strength and structural failure of rocks based on energy dissipation and energy release principles. Chin J Rock Mech Eng 24(17):3003–3010

Xie HP, Li LY, Peng RD, Ju Y (2009) Energy analysis and criteria for structural failure of rocks. J Rock Mech Geotech Eng 1(1):11–20. https://doi.org/10.3724/SP.J.1235.2009.00011

Zhang K, Zhou H, Shao J (2013) An experimental investigation and an elastoplastic constitutive model for a porous rock. Rock Mech Rock Eng 46(6):1499–1511. https://doi.org/10.1007/s00603-012-0364-5

Zhang S, Chen L, Lu P, Zhang Y (2021) Analysis of the energy and damage evolution rule for sandstone based on the particle flow method. Mech Time Depend Mater, 1–16. https://doi.org/10.1007/s11043-021-09499-9

Zhao H, Zhang C, Cao W, Zhao M (2016) Statistical meso-damage model for quasi-brittle rocks to account for damage tolerance principle. Environ Earth Sci 75(10):862. https://doi.org/10.1007/s12665-016-5681-7

Zhou ZB (2001) Principle of minimum energy consumption and its application. Science Press, Beijing ((**in Chinese**))

Zhu T, Chen J, Huang D, Luo Y, Li Y, Xu L (2021) A DEM-based approach for modeling the damage of rock under freeze-thaw cycles. Rock Mech Rock Eng 54(6):2843–2858. https://doi.org/10.1007/s00603-021-02465-4